PROTOTYPE ENGINE CONTROL SYSTEM DEVELOPMENT

By

Ping Mi

A THESIS

Submitted to
Michigan State University
in partial fulfillment of the requirements
for the degree of

MASTER OF SCIENCE

Mechanical Engineering

2012

ABSTRACT

PROTOTYPE ENGINE CONTROL SYSTEM DEVELOPMENT

By

Ping Mi

In order to improve the fuel economy and reduce exhaust emissions for automotive engines, many novel technologies need to be validated during engine dynamometer tests. This study focuses on developing a MotoTron based prototype engine control system for dynamometer applications. This work is motivated by the need for a flexible engine control system for various engines from single cylinder gasoline and diesel optical engines to multi-cylinder metal engines. The developed engine control system consists of a MotoTron ECU (engine control unit), a customized actuator drive box, and a host computer with LabVIEW GUI (graphic user interface). The host computer and the ECU communicate through CAN (control area network). The developed prototype engine control system was validated in the hardware-in-the-loop (HIL) simulation environment with a simplified engine model implemented in a dSPACE. The developed control system was utilized in many experiments such as optical engine fuel spray tests, gasoline and diesel engine combustion tests, and variable valve actuation tests.

In addition to the prototype engine control system development, an engine fuel rail pressure control system was also developed for diesel engines. Two robust controllers, H_2 and H_∞, were developed to regulate the common rail fuel pressure of a diesel engine, where the fuel injection was considered as the disturbance input and the fuel viscosity as the system parameter uncertainty. The sensor measurement noise was also taken into consideration in this design. The performances of the designed controllers were compared with a PI baseline controller through simulation study. The results show that the H_2 robust controller achieves the best performance.

ACKNOWLEDGMENTS

After one and half year study at MSU, I have got quite a list of people to express my appreciations. The completion of this thesis would be impossible without their continuous encouragement, help, and support.

First, I would like to thank my advisor, Dr. Guoming Zhu, who leads me into this new research area. Because of his excellent and patient guidance, I learned a lot during this master program. Also, he helped me built up my confidence with his continuous encouragement. I am really so grateful for everything he did for me.

I would also like to thank my committee members: Dr. Harold Schock, who always talks to me with a warm-heart smile and gives me his best suggestions; Dr. Jonguesn Choi, who is always very kind and willing to help me. Thank you for your helpful discussions and insightful comments during this thesis work.

In addition, my gratitude is sent to my research teammates and all the friends in our lab: Xuefei Chen, Shupeng Zhang, Jie yang, Andrew White, Peter Dolce, Xiaojian Yang, Zhen Ren, Yingxu Wang, Tao Zeng, Chao Cheng, Taotao Jin, Stephen Pace, Andrew Huijen, Tom Stuecken, Kevin Moran, and Aida Montalvo. I also would like to thank Gongda Power company for allowing me to use the engine test result in this thesis.

At last, I am also so grateful for my parents and my husband, for everything they did for me. They were always there no matter I was up or low. I just do not have enough words to express my appreciation and my love to them. Of course, this acknowledgement would be incomplete without mention my lovely daughter, Amy Chen, I wish her happy every day.

TABLE OF CONTENTS

LIST OF TABLES

LIST OF FIGURES

CHAPTER 1

INTRODUCTION

1.1 Background and Motivation

Increasing concerns about the global environmental change and energy shortage [1]-[5] drive the research and development of new automotive engine technologies. With more novel technologies developed for the automotive engines, advanced prototype engine control systems become more and more important [6]. Existing control systems for rapid prototyping and hardware-in-the-loop (HIL) simulations include dSPACE [7], Opal-RT [8], Electronic control units (ECUs) [9], and so on.

In this thesis, a low-cost MotoTron ECU based engine control system was developed [10]-[12]. ECUs have become a standard component in most vehicles since 1980s [13]. Nowadays, the capability of the ECUs has significantly increased. The ECU is no longer just used to control a single component, but also to control multiple devices through CAN (controller area network) communications, such as internal combustion engines, electrical motors, transmissions, ABS (anti-lock brake system), and so on [14]. Most production ECUs are programmed in the "C" language and Matlab/Simulink, but for rapid prototype development, Matlab/Simulink is more commonly used [15]. The engine control system in this research was developed in a MotoHawk environment [10]-[12]. The algorithm consists of five engine operation modes. In each mode, different fuel and spark timings are calculated. In addition, the engine control system developed in this thesis also includes a LabVIEW GUI control interface

[16], so that users can tune the control parameters in real time. The MotoTron controller and the host computer communicate through a CAN link.

In this thesis, in addition to the prototype engine control system development, an engine fuel rail pressure control system was also developed for diesel engines. Common rail diesel fuel system was invented by BOSCH in 1978 [17]. Before that, fuel injection systems were cam-driven. The fuel pressure varies as the engine speed changes, which results in low fuel injection qualities [18]. Common rail fuel systems generally include a fuel pump, a fuel rail, and several fuel injectors. The fuel injection system can operate at very high pressure with a flexible electronic control of fuel delivery, injection timing, injection pressure and rate of injection by multiple injection strategies [18]-[19]. By controlling these parameters, the common rail fuel system is capable of achieving low exhaust emissions and high engine performance, as well as low engine combustion noise, and so on [20]-[24].

Many studies have been conducted for common rail fuel systems modeling and control. Reference [25] developed a mathematic common rail system model based on physical laws. Reference [26] developed a common rail fuel system model based on energy principle. Reference [27] presented a very detailed model for a common rail fuel system. However, their model comprises of some partial differential equations, and is difficult to be used in control system design and validation. This thesis presents a control oriented common rail fuel system model, and two robust controllers, H_2 and H_∞ were developed to control the fuel rail pressure based on the developed model.

1.2 Research Overview

1.2.1 Engine management system development

In this thesis, an engine control system based upon the MotoTron controller was developed. It was originally designed for a single cylinder optical diesel engine and then was modified to control a 4-cylinder gasoline engine. Figure 1-1 shows the engine control system architecture. Each function block in this control system is described in detail in this thesis. In addition, the control algorithm is also introduced followed by several application results.

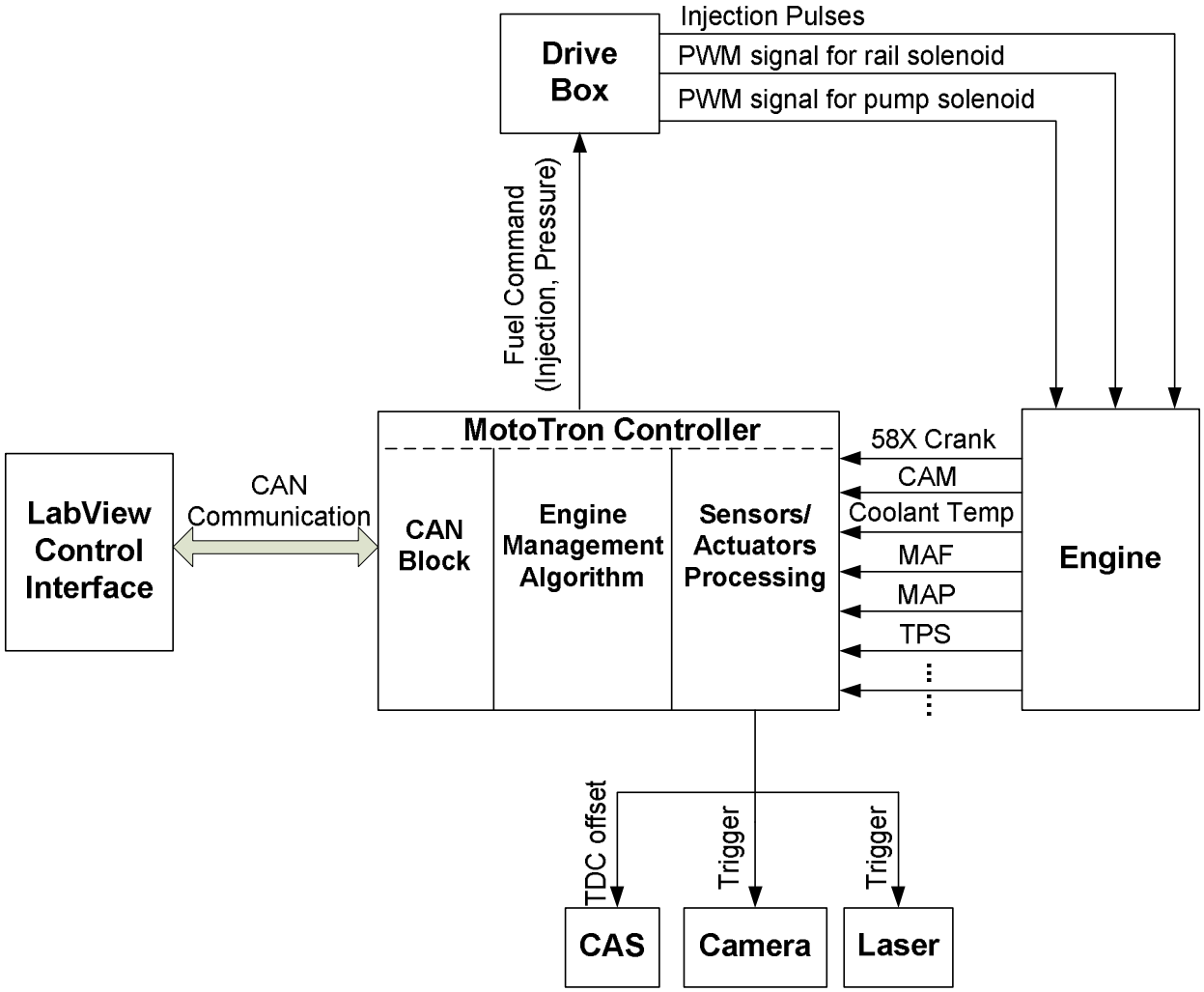

Figure 1-1 Engine control system architecture for a diesel engine

1.2.2 Advanced controller design for a common rail system

In this thesis, a common rail fuel system was modeled as a second order system, which took into consideration of fuel injection disturbance, sensor noise, and the fuel property uncertainty. Two robust controllers are proposed for regulating the common rail pressure as steady as possible. The two controllers were then evaluated through simulations by comparing them with a baseline PI controller. Note that, each controller was optimized with respect to its performance. Figure 1-2 is the flow chart used to acquire the controllers.

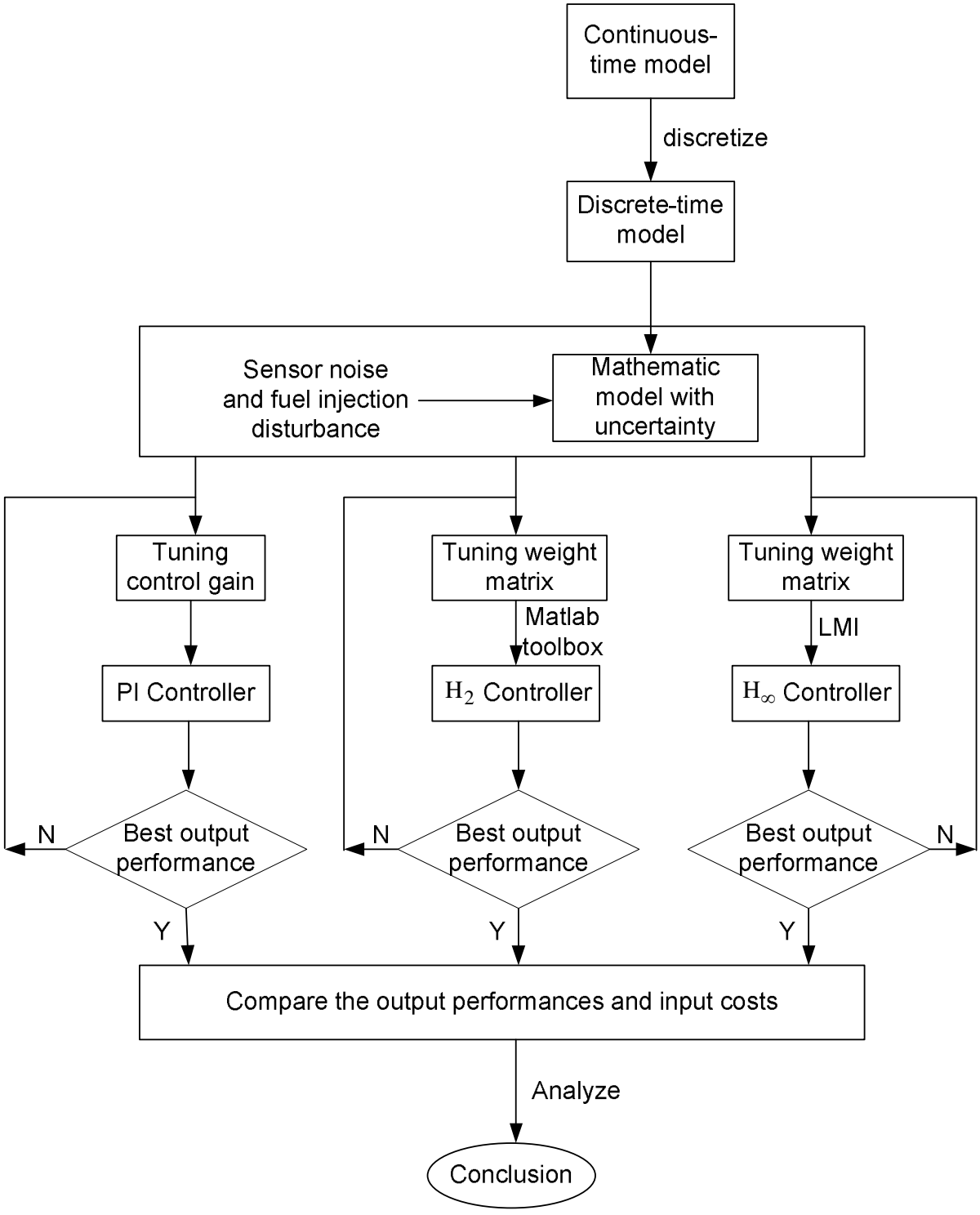

Figure 1-2 Flow chart to acquire controllers for common rail system

1.3 Organization

The material presented in this thesis is organized into three chapters. In Chapter 2, an engine control system that has five control modes was developed based upon a MotoTron ECU, the control system including system architecture and algorithm structure are described in detail. Also, the control system was validated through hardware-in-the-loop (HIL) simulations and some dynamometer tests, the test results are presented. In Chapter 3, a common rail fuel system and the corresponding discrete-time second order system are introduced, and two robust controllers were designed to regulate the fuel rail pressure. The simulations were conducted to compare the performances of the two robust controllers and a baseline PI controller. In Chapter 4, conclusions and future work are addressed.

CHAPTER 2

PROTOTYPE ENGINE CONTROL SYSTEM DEVELOPMENT

2.1 Introduction

Fast developing engine technologies require flexible, rapid prototype engine control systems. In this thesis, an engine control system was developed based upon a MotoTron ECU. The control system consists of three major blocks, which are I/O definition, engine management system, and CAN communication. The engine management system defines the Engine Status in five modes. The engine control system also consists of a host computer. The human control interface was developed using LabVIEW software.

The developed control system was validated through hardware-in-the-loop (HIL) simulations [28]. HIL is a standard tool for developing electronic or mechanical automotive components. A single component or even a entire vehicle can be replaced by mathematical models running in real time on small and cost-effective hardware platforms, while other components which need testing or are just part of the test setup, are connected to the simulator in a closed loop configuration [29]. In this HIL simulation, a simplified engine model was developed in dSPACE. The MotoTron ECU sends the control commands to the dSPACE engine model through the CAN communication, while reading back the engine sensor signals including crank signal, CAM signal, mass air flow (MAF) signal, throttle position signal (TPS), idle valve position, coolant temperature, and so on.

After the HIL simulation validation, the developed engine control system was used for several engine projects, such as the optical diesel engine project, the small gasoline engine project, as well as a variable valve actuation (VVA) system development project [30]-[32]. High speed imaging tests on the optical engine can help the analysis of the fuel spray, mixture formation, combustion flame development, and emission formation [33]-[34]. This engine control system provides two trigger pulse signals for high speed imaging tests. They can be used for high speed camera and the laser source. VVA (variable valve actuation) systems have many advantages, including improved fuel economy and reduced exhaust emissions. This engine control system also includes a VVA block. It provides the valve open and close timing, as well as the valve lift control signals to the VVA actuator. This thesis presents several engine dynamometer experiment results with the use of the developed engine control system. It is found that the developed engine control system meets all the requirements of these applications.

2.2 Engine Control System Development

2.2.1 System architecture

In this development, the engine control system consists of a MotoTron production ECU (engine control unit), a customized actuator drive box, and an engine control host computer with LabVIEW GUI (graphic user interface). The ECU and the host computer are communicated through CAN (control area network) by a National Instrument (NI) Hi-Speed USB device (NI USB-8473). Figure 2-1 shows the system architecture diagram.

The MotoTron production controller used in this system has 33 analog input channels, 3 digital input channels and several output channels. The controller is synchronized based upon the 58X teeth crank sensor and the single pulse cam sensor. In addition, MotoTron provides a TDC

(top dead center) offset calibration for the users to synchronize the virtual logic TDC of MotoTron with the physical TDC of the engine. This control system provides users with a constant pulse signal delivered at virtual TDC of MotoTron for the system synchronization application. Two trigger pulse signals are specifically designed for optical engine tests. One is for high speed camera, and the other is for the external laser source. These two trigger pulses can help synchronize the captured images with the engine combustion data (e.g., in-cylinder pressure signal) logged in the combustion analysis system (CAS).

The engine control drive box was designed for multiple applications. It is not only able to drive the ignition dwell current up to 20A for a gasoline engine (since the MotoTron control module does not include any ignition driver), but it is also able to drive fuel injectors for diesel engines. In addition, this drive box also has two PWM channels, which can be used to drive the fuel pump return control solenoid, and the fuel rail return solenoid.

The host computer communicates with the engine controller through CAN using an NI USB-CAN plug-in device. The LabVIEW GUI was developed for real time control of the engine. Many engine signals can be displayed on this GUI. In the meanwhile, a calibration LabVIEW page, which consists of many control parameters, can be used to tune the engine control system on-line in real time.

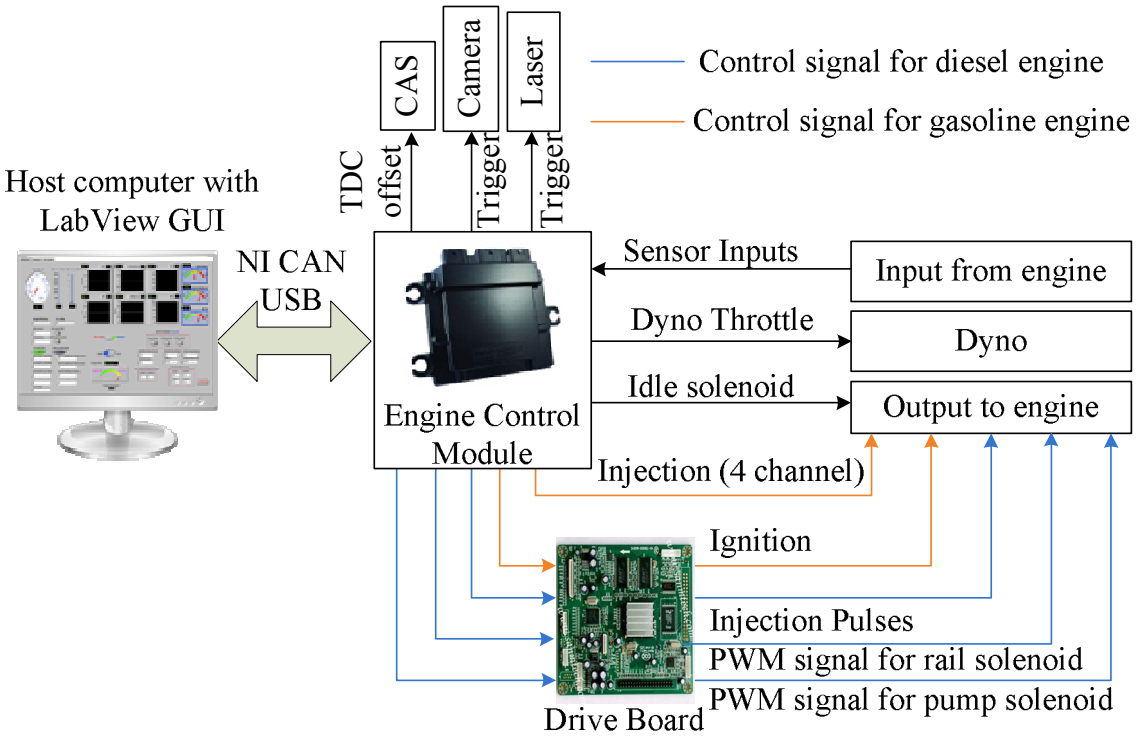

Figure 2-1 Engine control system architecture(For interpretation of the references to color in this and all other figures, the reader is referred to the electronic version of this thesis)

2.2.2 Engine control algorithm structure

The engine control system algorithm was developed in Simulink using MotoHawk software that provides a common tool for auto-code generation, modeling, control system design and I/O functions, so that the engine control system algorithm can be developed efficiently and coded automatically from Matlab/Simulink to the C codes that run in the MotoTron production controller [13]. The whole control algorithm consists of three major parts as shown in Figure 2-2: 1) Sensor and actuator signal processing; 2) Engine management system (EMS); 3) CAN communications.

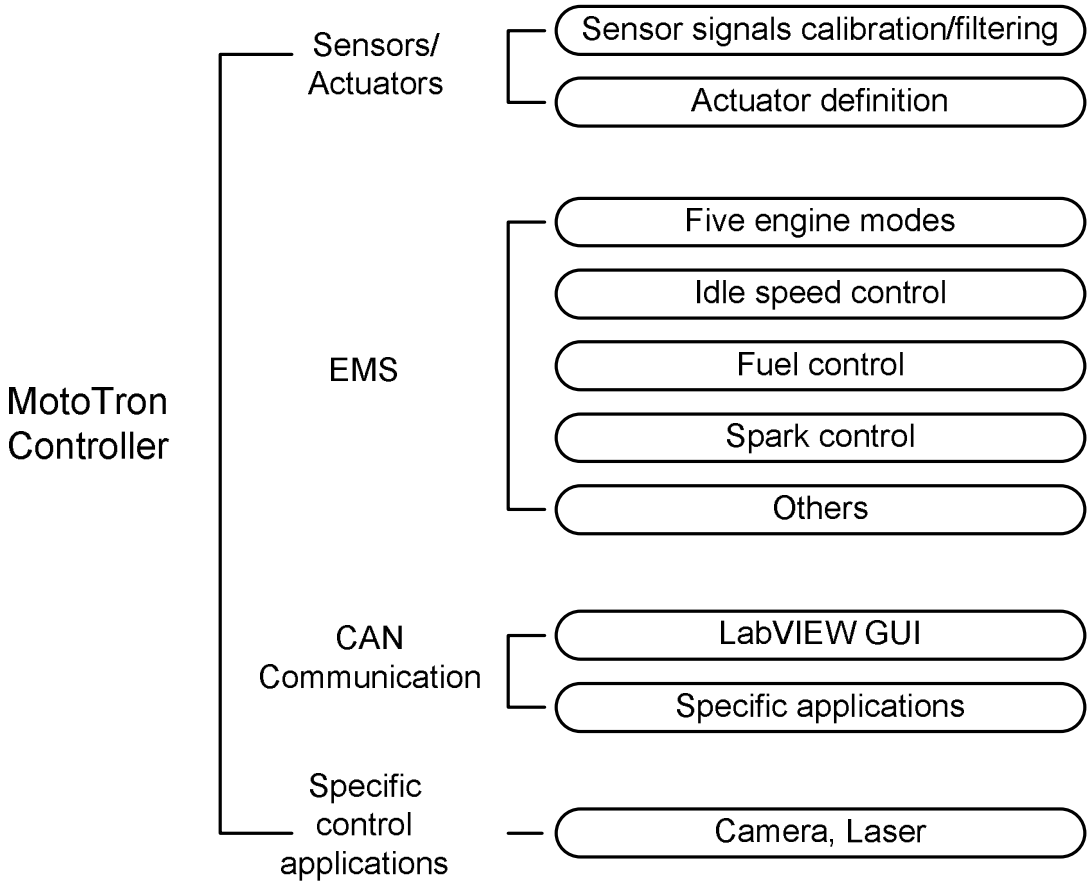

Figure 2-2 Engine control algorithm structure

2.2.3 Sensor and actuator signal processing

Sensor and actuator signal processing are always an important part of the control system development work, especially for automotive engines, which usually have dozens of sensors and actuators. Table 2-1 and Table 2-2 list the actuators and sensors included in this control system, as well as their signal type definition.

Table 2-1. Output control signal definition.

	Signal Definition	Type
1	Injector #1	13.5V (on-off pulse)
2	Injector #2	13.5V (on-off pulse)
3	Injector #3	13.5V (on-off pulse)
4	Injector #4	13.5V (on-off pulse)
5	Ignition #1,4 (waste spark)	13.5V (on-off pulse)
6	Ignition #3,2 (waste spark)	13.5V (on-off pulse)
7	Engine idle solenoid	PWM (2A max)
8	Intake valve control (high open) #1	TTL
9	Intake valve control (high open) #2	TTL
10	Exhaust valve control (high open) #1	TTL
11	Exhaust valve control (high open) #2	TTL
12	Valve lift reference	PWM (0 ~ 5 V)
13	Thermostat solenoid	PWM (2A max)

Table 2-2. Input sensor signal definition.

	Signal Definition	Type
1	Crank position pulse	60-2, TTL
2	Cam position pulse	Single tooth, TTL
3	Manifold air pressure	0 ~ 5 V
4	Manifold air temperature	0 ~ 5 V
5	Throttle position	0 ~ 5 V
6	Air-to-fuel ratio	0 ~ 5 V
7	Mass air flow	0 ~ 5 V
8	Coolant temperature	0 ~ 5 V
9	Oil pressure	0 ~ 5 V
10	Engine load percentage	0 ~ 5 V
11	Combustion Analysis System	TTL
12	Camera and Laser	TTL

In this engine control system, the digital signals are processed in the crank based event mode, and all the analog signals are updated with a 5 ms fixed sample period. Filters in Figure 2-3 are used for the analog signals, and the filter coefficient, as well as the filter duration can be tuned through the host computer. Each sensor is calibrated based upon its characteristic curves.

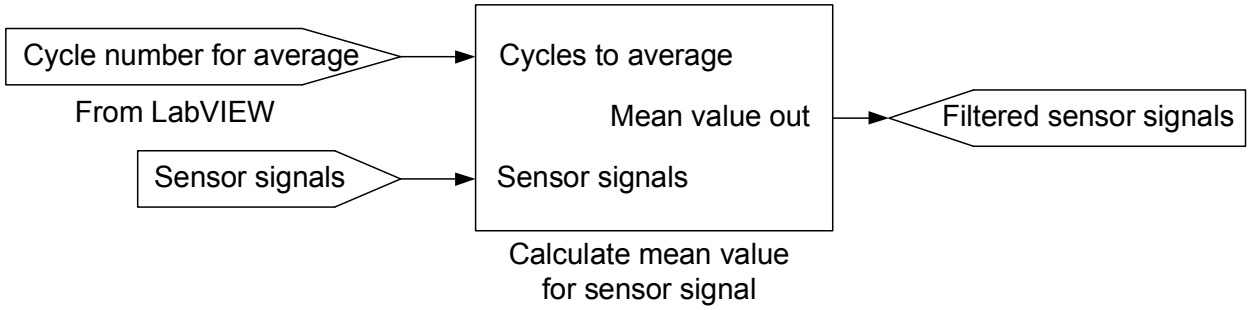

Figure 2-3 Analog signal filter

For the actuators, some of them are operated in the time based mode, such as the idle valve, the thermostat, fuel rail and fuel pump solenoids, and the rest work in the crank based event mode, such as fuel injector, ignition coil, and so on. It is important to define the types of the actuator signals before they are used. In this engine control system, the injection signals are TTL type signals that are able to either drive the current-based injector driver directly, or work as a trigger pulse to the diesel injector driver circuit in the drive box. The ignition signals are also a TTL type signals. Besides the fuel injection signals and the ignition signals, this control system also provides four TTL control signals for a specific customer (Gongda Power) to be used as four variable-valve-actuation control reference signals (two intake and two exhaust valves for cylinder 4). In addition, several PWM (pulse width modulation) signals were generated for fuel rail solenoid control, fuel pump solenoid control, electrical thermostat control, and the valve lift signal reference.

Figure 2-4, Figure 2-5, and Figure 2-6 shows the I/O connection diagrams. Specifically, Figure 2-4 is the power connection for ECU. Figure 2-5 shows the connections for sensors. And the connections for actuators are presented in Figure 2-6.

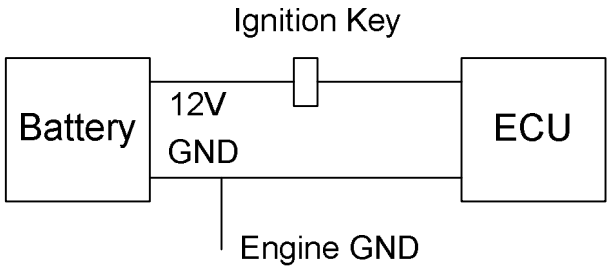

Figure 2-4 ECU power connection

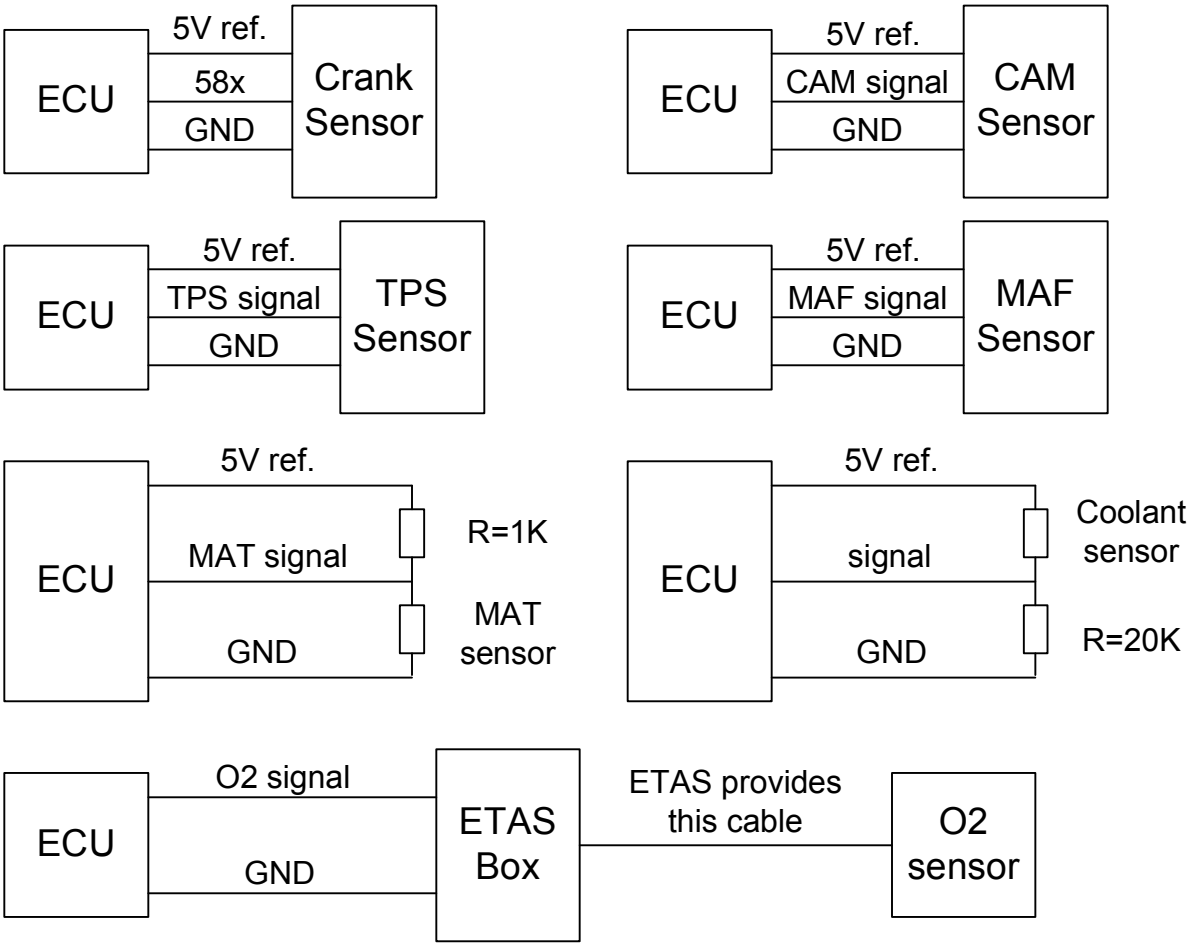

Figure 2-5 Sensor signals to ECU

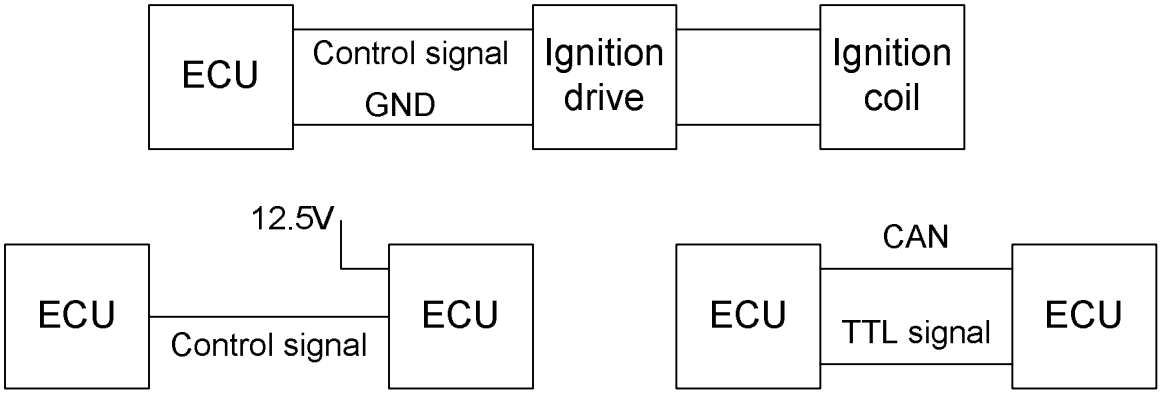

Figure 2-6 Control signals from ECU to actuators

2.2.4 Engine management system

The engine management system is the core of the whole engine control system algorithm. This thesis lists several of the important modules, such as engine working modes definition, idle speed control, fuel control, spark control, and so on.

2.2.4.1 Engine operation modes

In this control system, the engine operation is defined by five working modes. They are

- stall mode (*engine_status_flag* = 01)
- crank mode (*engine_status_flag* = 02)
- idle mode (*engine_status_flag* = 03)
- running mode (*engine_status_flag* = 04)
- shut down mode (*engine_status_flag* = 05)

The *engine_status_flag* is used to indicate the current engine status. Figure 2-7 shows the status flow of the engine operation modes. The engine operation modes are mainly decided based upon the engine speed and the engine throttle position. Note that, hysteresis are applied for all decision making thresholds. A shut down button is provided in the LabVIEW GUI which requires to mandatory shut down the engine by disabling all the control commands regardless of

the current engine status. The stall mode is designed for engine system start preparation. For example, the idle valve is initialized to a pre-calibrated position during this operation mode. Fuel begins to be delivered when the engine enters the crank mode. In this operation mode, rich air-to-fuel ratio (AFR) with respect to the coolant temperature is used for the engine to overcome the large crank resistant friction. In general, the crank mode is very short. When the engine speed exceeds a threshold, the engine mode switches to idle mode. In idle mode, the AFR will ramp to the desired level defined in a lookup table. The AFR lookup table is also function of the coolant temperature. When the coolant temperature exceeds a threshold, or the engine runs for enough long time, the AFR will ramp to the stoichiometric AFR (14.6) and the system starts running in closed-loop AFR control mode. During idle mode, several closed-loop controls are used, such as idle speed control, and AFR control. When the throttle position signal (TPS) is greater than a certain value, the engine starts to run in running mode. In this mode, the AFR is still controlled in closed-loop mode, while the spark is based upon a lookup table as function of engine speed and the engine load. The idle valve position is kept at its current position.

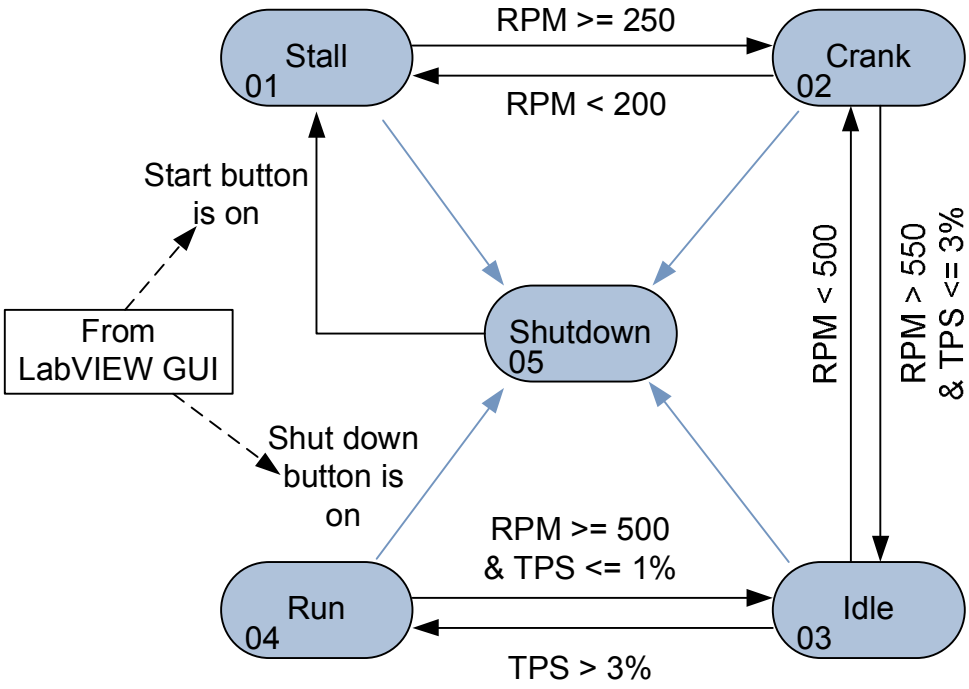

Figure 2-7 Engine working modes transition diagram

2.2.4.2 Fuel control

In the engine management system, the desired AFR is based upon the output of a lookup table as function of the coolant temperature. The fuel injection quantity, or corresponding fuel pulse width, consists of two parts. One is base fuel quantity based upon the desired AFR and the mass air flow (MAF) measured by the MAF sensor, and the other is due to the closed-loop control correction, which is mainly based upon the feedback AFR sensor signal. The total fuel quantity is calculated as

$$m_f = \frac{m_a}{AFR} + \Delta m_f \tag{2.1}$$

where m_a is the intake air mass calculated by

$$m_a = \frac{\dot{m}_{MAF}}{\frac{2N}{\tau} \times n} \tag{2.2}$$

where $\dot{m}_{MAF}$ is the mass air flow rate measured by MAF sensor; N is the engine speed; n is the number of the cylinders; and τ is the number of strokes. The Δm_f is the closed-loop fuel correction, it is calculated by

$$\Delta m_f = \left(\frac{K_I}{s} + K_P \right) \left(\phi - AFR_d \right) \tag{2.3}$$

where K_P and K_I are the proportional and integral gains of the AFR PI controller, respectively; ϕ is the oxygen sensor signal; and AFR_d is the desired AFR. Note that, the closed-loop air fuel ratio control is only enabled when AFR_d is equal to the stoichiometric AFR (14.6).

In addition, the LabVIEW GUI has an option to enable or disable the closed-loop AFR control, because sometimes, users might just want to use the open-loop fuel control and manually set up a fuel injection pulse. Figure 2-8 is the closed-loop air fuel ratio control.

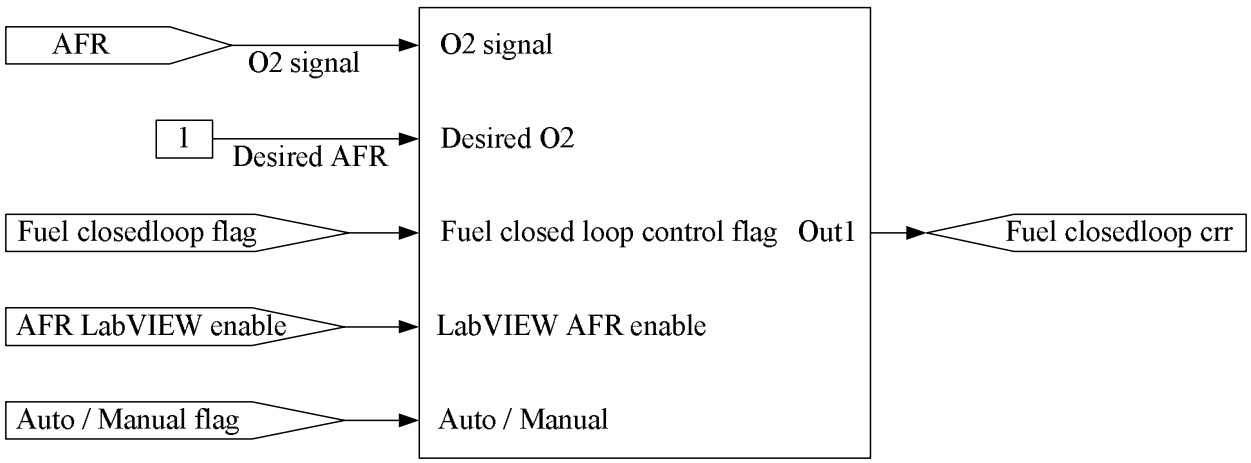

Figure 2-8 The closed-loop air fuel ratio control

The fuel quantity is then converted into the fuel pulse width based upon the fuel injector characteristic calibration curve. The fuel injection timing also has two options. Users can either

choose using the lookup table values, or manually set the injection timings through the host computer. In addition, this control system provides multiple injection option including pilot injection, main injection, and post injection. Each of them can be defined in the LabVIEW GUI.

2.2.4.3 Spark control

The spark control in this engine control system is based upon the output of a lookup table as function of engine speed and load. While in the crank and idle modes, the spark timing table is a function of the coolant temperature. In addition, a proportional spark timing control is used in the idle mode to have fast engine torque regulation and to have smooth engine idle speed. Lastly, a spark offset is provided in the LabVIEW GUI so that it can be manually tuned by the users for the control flexibility.

2.2.4.4 Idle speed control

The desired idle speed is also based upon the output of a lookup table as function of the coolant temperature. Like the fuel pulse width and the spark control, a similar option was also provided for users to manually set the desired idle speed in the LabVIEW GUI. As soon as the engine status indicates that it is in the idle mode, the closed-loop idle speed control is turned on. A proportional and integral controller (PI) is utilized to regulate the engine speed close to the desired speed by adjusting the idle valve position and the idle spark P (proportional) controller. Figure 2-9 shows the whole structure of the idle valve control. Note that, the gain scheduling scheme is used for the idle valve PI controller.

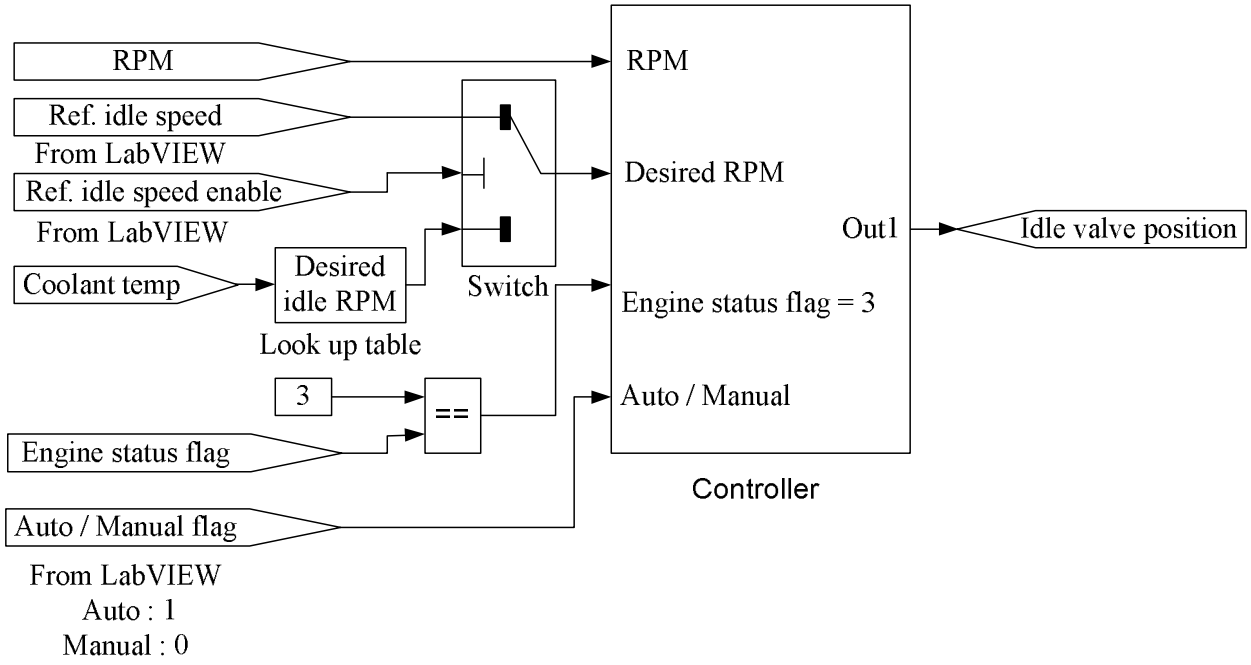

Figure 2-9 Idle speed control

2.2.4.5 Others

In addition to the above mentioned modules, this control system also has an over speed protection function. When the engine speed exceeds a set limit, the control system will cut off the fuel to protect the engine. Also, this control system provides a PWM control signal to control the electrical thermostat valve with respect to the coolant temperature. Figure 2-10 shows the flow chart of electrical thermostat control. In addition, several TTL output signals are provided in this control system. They are designed specifically for a variable valve actuation (VVA) system development engine. These TTL signals are used as the synchronization signals for opening and closing the intake and exhaust valves that are actuated by a hydraulic control system instead of the traditional CAM shaft, and the valve lift and timing signals are sent through CAN protocols.

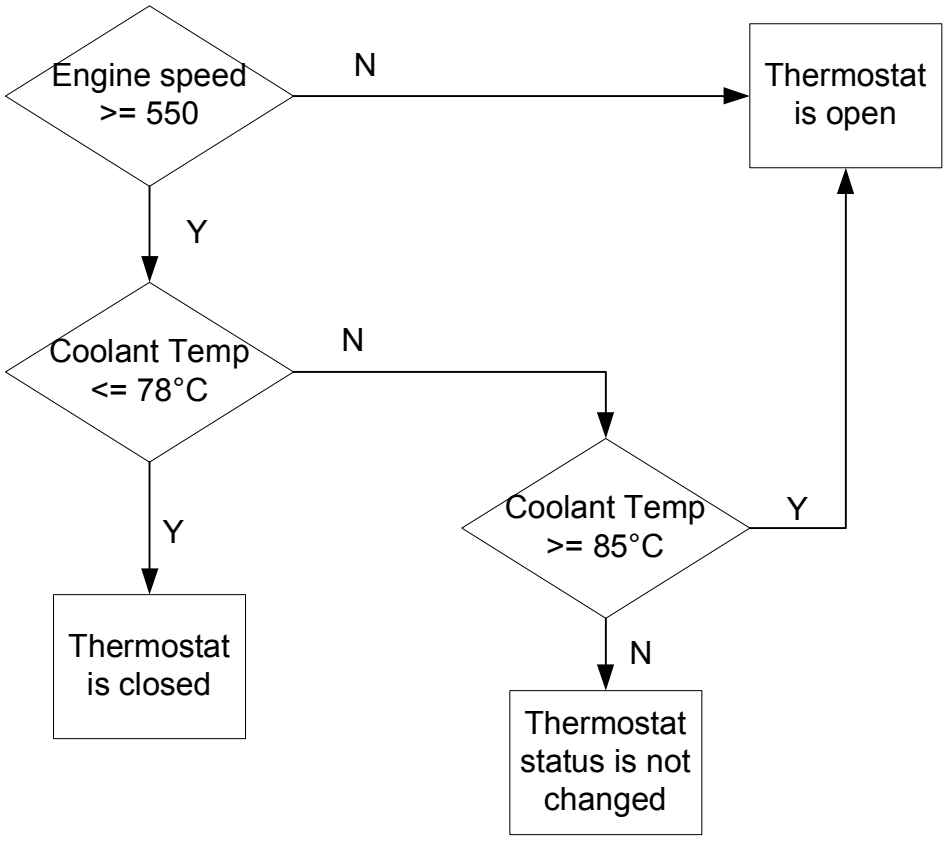

Figure 2-10 Flow chart of electrical thermostat control

2.2.5 CAN communication

CAN communication is also a very important part of the engine control system. The controller communicates with other devices through the CAN link as shown in Figure 2-11. The engine controller send the signals, such as engine speed, AFR, coolant temperature, delivered fuel pulse, delivered spark, to display in the LabVIEW GUI, while reads the control commands from the host computer. The CAN link between the MotoTron controller and the host computer uses a NI high-speed USB cable. This system also includes a CAN channel for the VVA control system. The control commands are sent to the VVA controller through the CAN link, while several TTL signals are used together for the VVA control as synchronization signals. In addition, a third CAN channel was added to communicate with the dSPACE HIL simulation

system, where a simplified engine model was developed for the hardware-in-the-loop (HIL) simulation so that the developed control system can be validated on the bench.

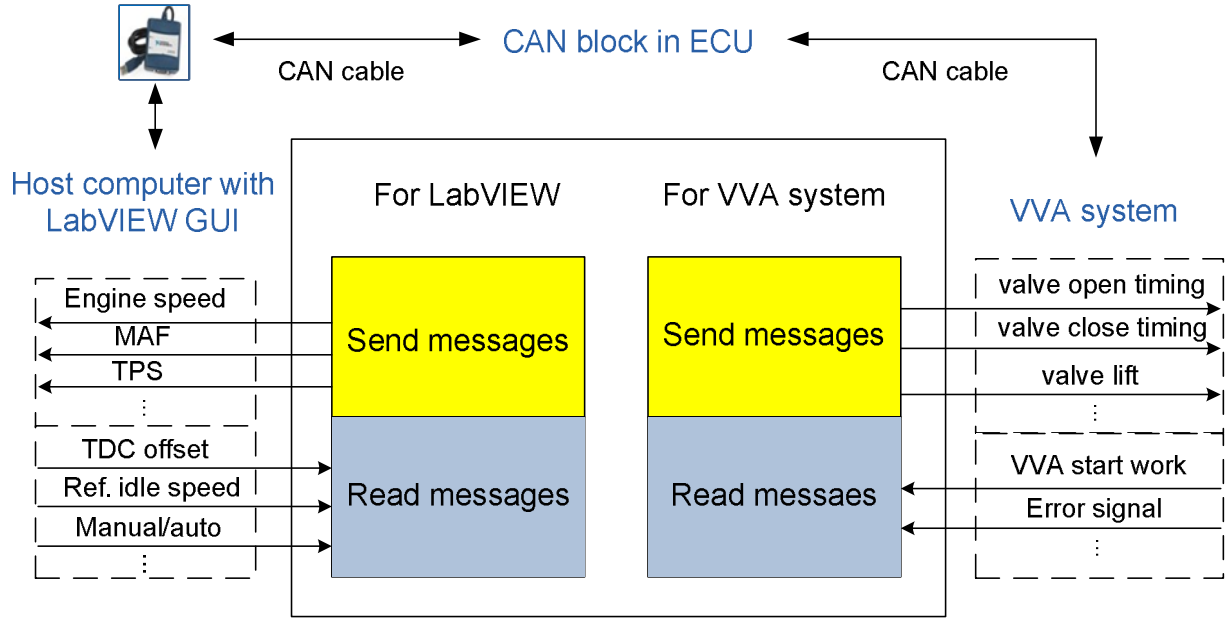

Figure 2-11 CAN communication

2.3 LabVIEW GUI Development

The host engine control computer runs under NI LabVIEW and generates a GUI. The motivation for using the LabVIEW GUI interface was to monitor the engine status, display sensor signals and the control parameter values, but most importantly, to provide real time control commands and parameter calibrations to the engine control system. The LabVIEW interface consists of two parts, one page includes all the sensor parameters and some important control commands, as well as part of the calibrations, while the other page lists of all other calibrations.

2.3.1 LabVIEW GUI main monitoring page

The first work in developing the GUI was to decide the parameters to be monitored in the GUI, the parameters to be calibrated in real time, and the format should be displayed. In this control system, both digital and analog display formats are used to display most parameters. For example, the idle valve position is shown as a percentage in a digital number and in a waveform graph. The advantage of the waveform graph is that it shows the history of the change of the signal. The main monitoring page of the developed LabVIEW GUI shows in Figure 2-12.

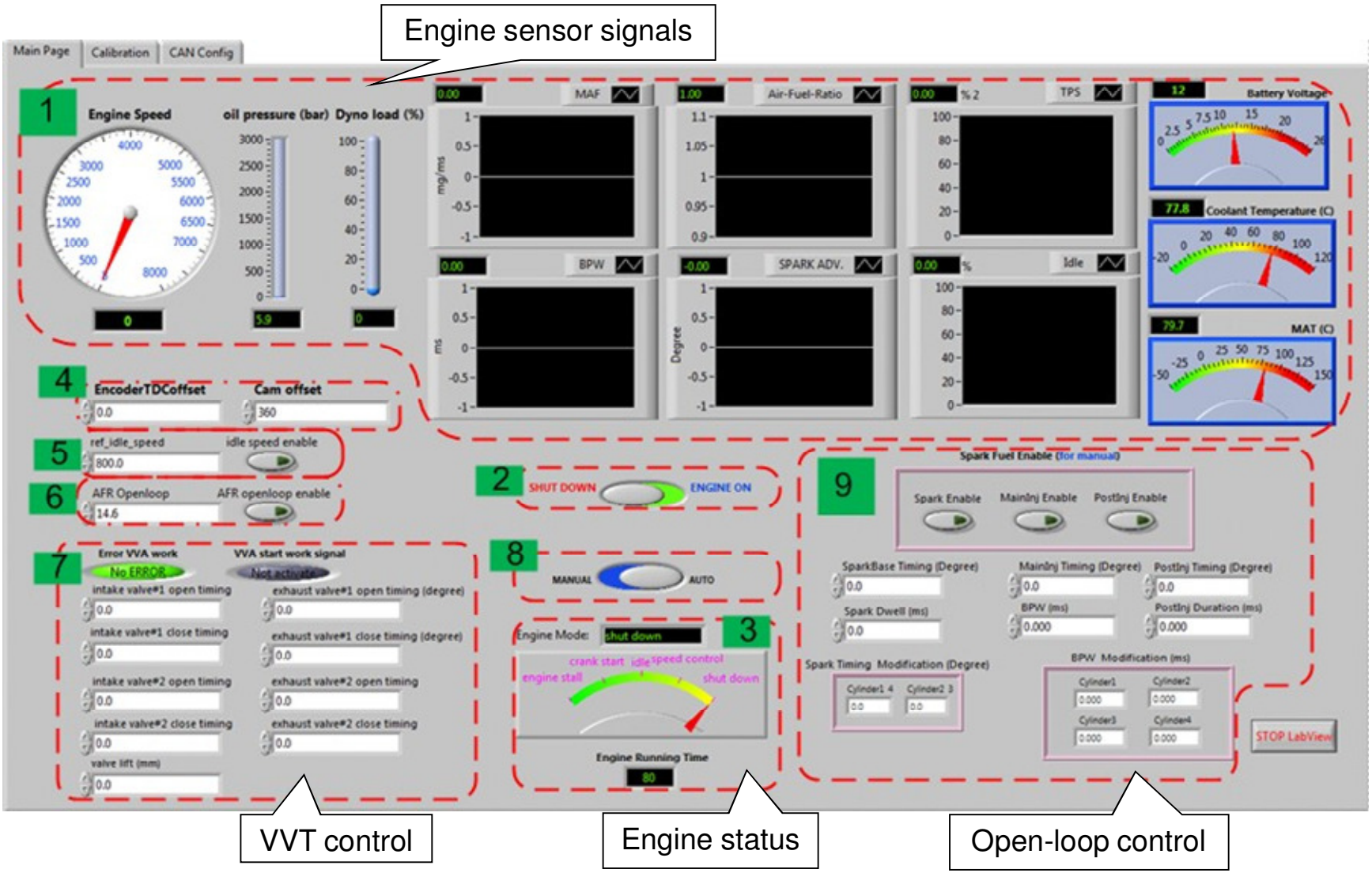

Figure 2-12 LabVIEW GUI main page

This page mainly consists of nine parts according to different functions, and each part is circled by a dotted red line. The first part shows all the monitored sensor signals, such as engine speed, throttle position, intake mass air flow, idle valve position, etc. The engine control commands and parameters are mainly included in parts 2 to 6. The seventh part is specifically designed for the variable valve actuator development project. Two VVA signals are displayed in this part. Four sets of opening and closing timing control of the two intake valves and two exhaust valves, respectively, were designed to provide the crank-synchronization control signals for the VVA controller. In addition, this LabVIEW GUI provides an option for users to switch the engine control to the manual mode as shown in part 8. In this manual mode, the fuel and spark control parameters can be manually set in part 9.

2.3.2 LabVIEW GUI calibration page

Figure 2-13 shows the calibration page. A few important control parameters can be calibrated in real time through this page. For example, the proportion gain, the integral gain, and the integral duration can be calibrated for idle control valve, idle fueling, and spark timing, respectively. Note that, the PI controllers developed in this control system use gain scheduling schemes, and the proportional gains and the integral gains in this LabVIEW GUI are multiplied by lookup table based gains preloaded in the MotoTron controller. In addition, the sensor filtering parameters are also very important. They are shown in part 2 in this figure. Part 3 in this plot shows several other important calibration parameters such as initial idle valve position, AFR transition step from the crank AFR to the idle crank AFR, a fuel gain which is considered as a compensation for the volumetric efficiency.

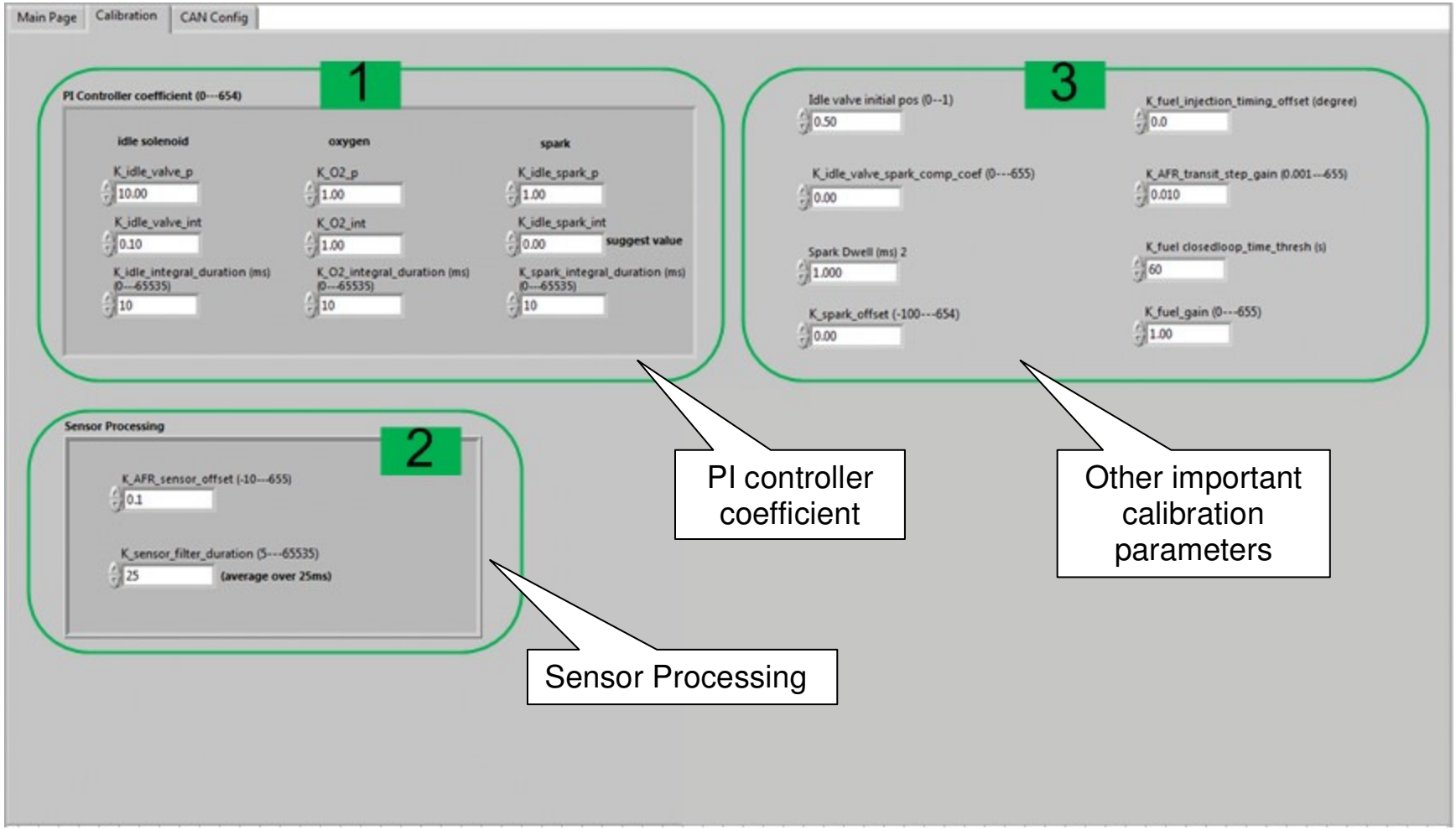

Figure 2-13 LabVIEW GUI calibration page

2.4 HIL Simulation

Utilizing an appropriate control-oriented engine model, an HIL simulator, such as the dSPACE engine simulation system, is capable of providing various engine output signals based upon the control signals provided by the engine controller at different engine operational conditions [35]. The developed engine control system was validated through HIL simulations before it was implemented for engine dynamometer tests. Figure 2-14 HIL simulation diagram of engine control system shows the HIL simulation diagram of the engine control system. It consists of a host computer with LabVIEW GUI, a MotoTron controller and a dSPACE loaded with a simplified engine model. The simplified engine model that runs in the dSPACE sends sensor signals to the controller through A/D channels or CAN communications, and receives the control parameters from the MotoTron controller through CAN link.

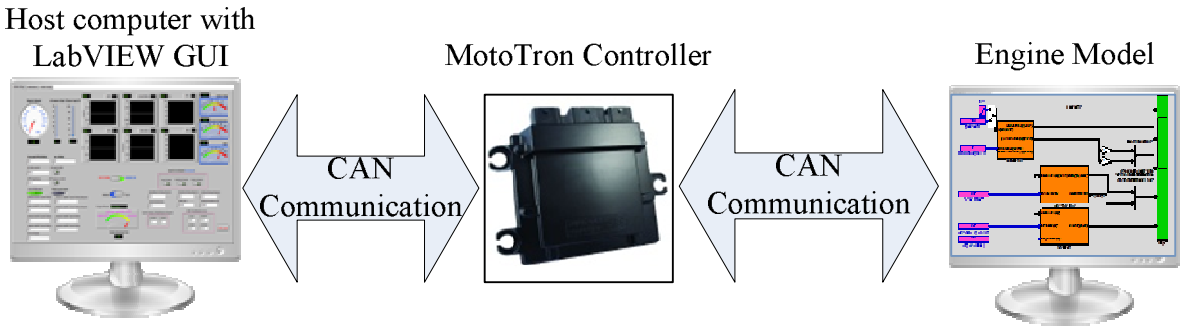

Figure 2-14 HIL simulation diagram of engine control system

Figure 2-15 shows an engine start up HIL simulation flow chart, Figure 2-16 is the corresponding HIL simulation result.

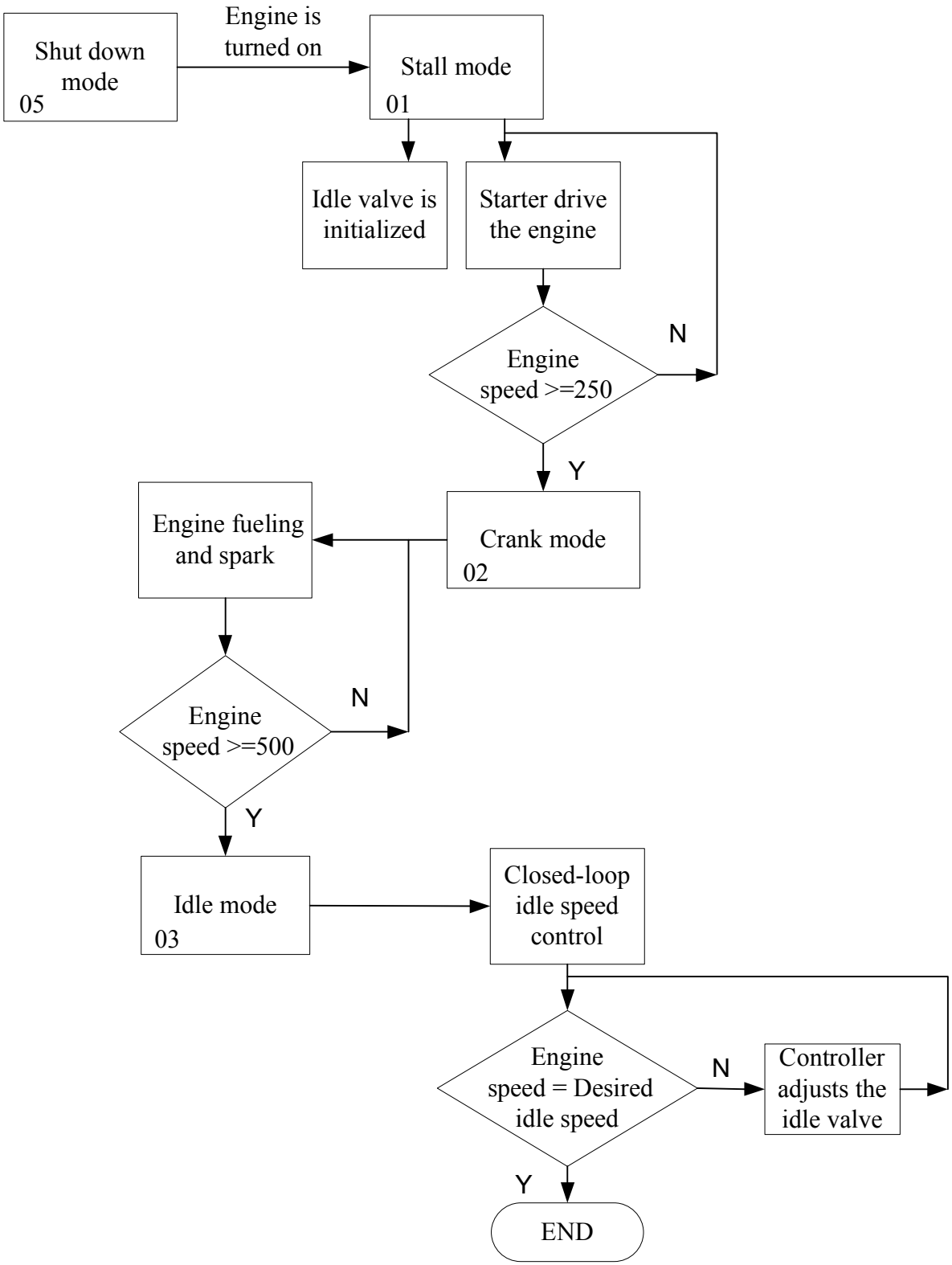

Figure 2-15 Engine start up HIL simulation flow chart

The initial idle valve position was set to 35%. The engine was turned on at the 2nd second. It can be observed that the engine status was switched from shut down mode to the stall mode immediately. As a result, the idle valve was initialized to the predefined position. When the starter drove the engine speed above a calibrated threshold, the engine operation mode was shifted into mode 2, the crank mode. Both the fuel and spark were delivered starting at 3.5 seconds. The engine entered into the idle mode when the engine speed exceeded 500 rpm. In the idle mode, the closed-loop idle speed control was turned on. The controller adjusted the idle valve to regulate the engine speed to the desired speed. In this case, the desired engine speed was set at 800 rpm. It can be found that the actual speed tracked the desired speed pretty well. The HIL simulation results also demonstrated that the designed algorithm works as expected.

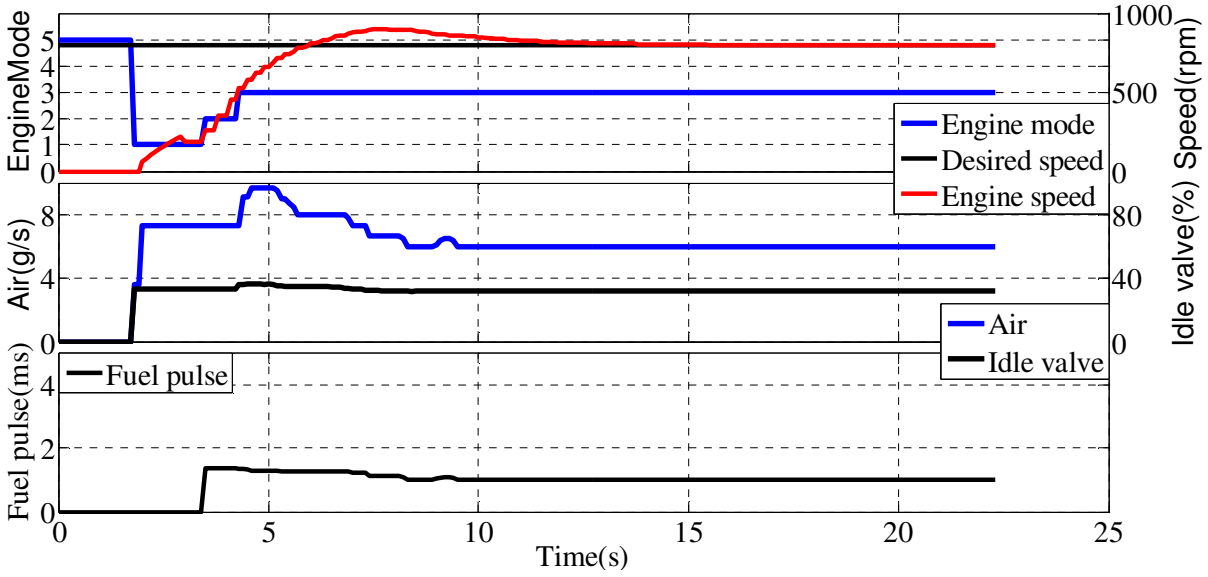

Figure 2-16 Engine start up HIL simulation result

2.5 Engine Dynamometer Applications

This engine control system has been used for several engine projects. The first project was a single cylinder, direct injection (DI) optical diesel engine. The specifications of the engine

are listed in Table 2-3. The injector is a Siemens piezo injector using a 6-hole nozzle with holes of 0.185mm with a cone angle of 154 degrees. Figure 2-17 shows the engine and the dynamometer control setup. A baseline CAS (Combustion Analysis System) from AND Technologies was used to record the engine combustion data. The MotoTron ECU was synchronized by calibrating the TDC offset through the LabVIEW GUI.

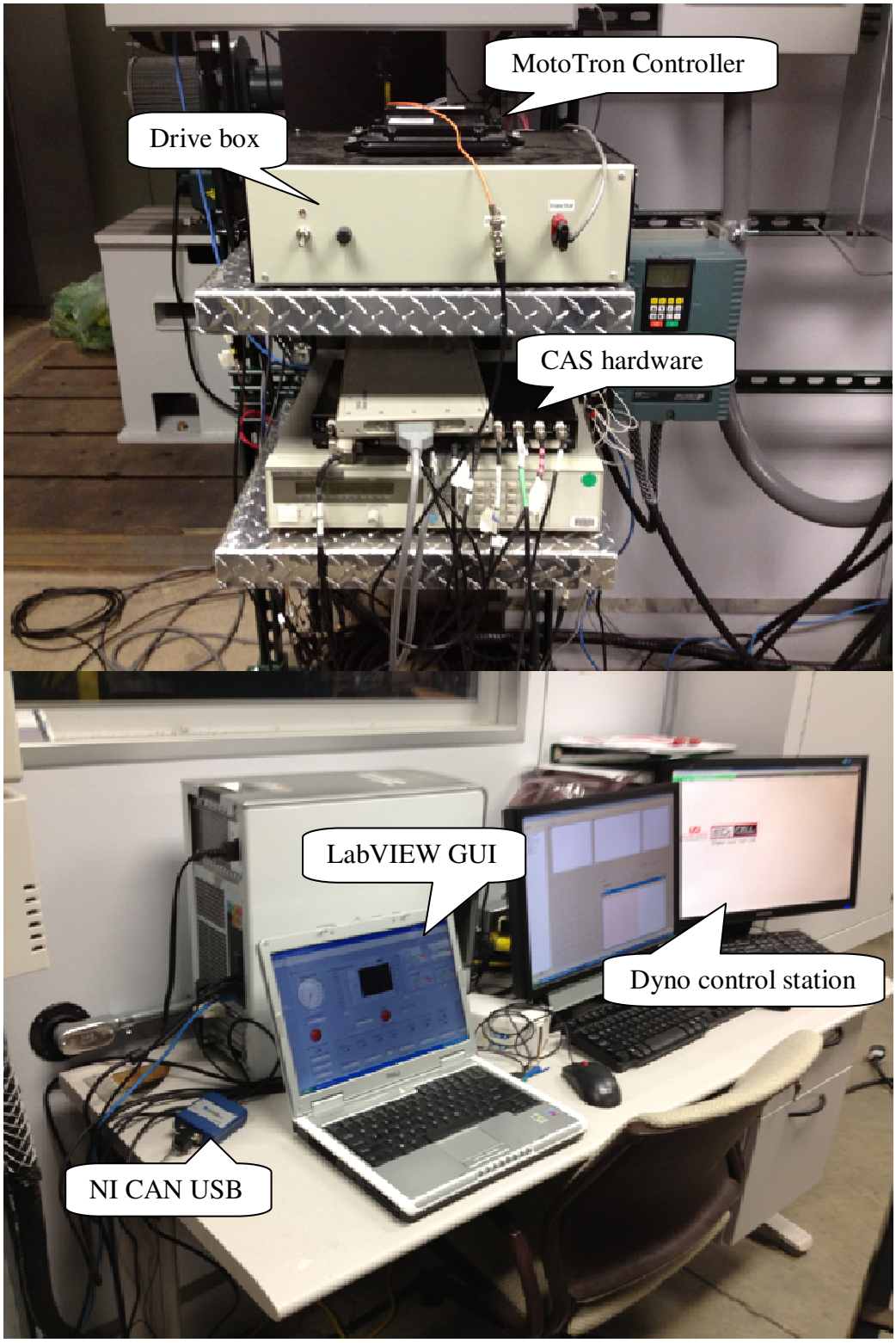

Figure 2-17 Engine dynamometer setup

Table 2-3. Engine specifications.

Bore	95	mm
Stroke	105	mm
Displacement	0.75	liter
Cylinder Number	1	unit
Compression Ratio	17:1	unit

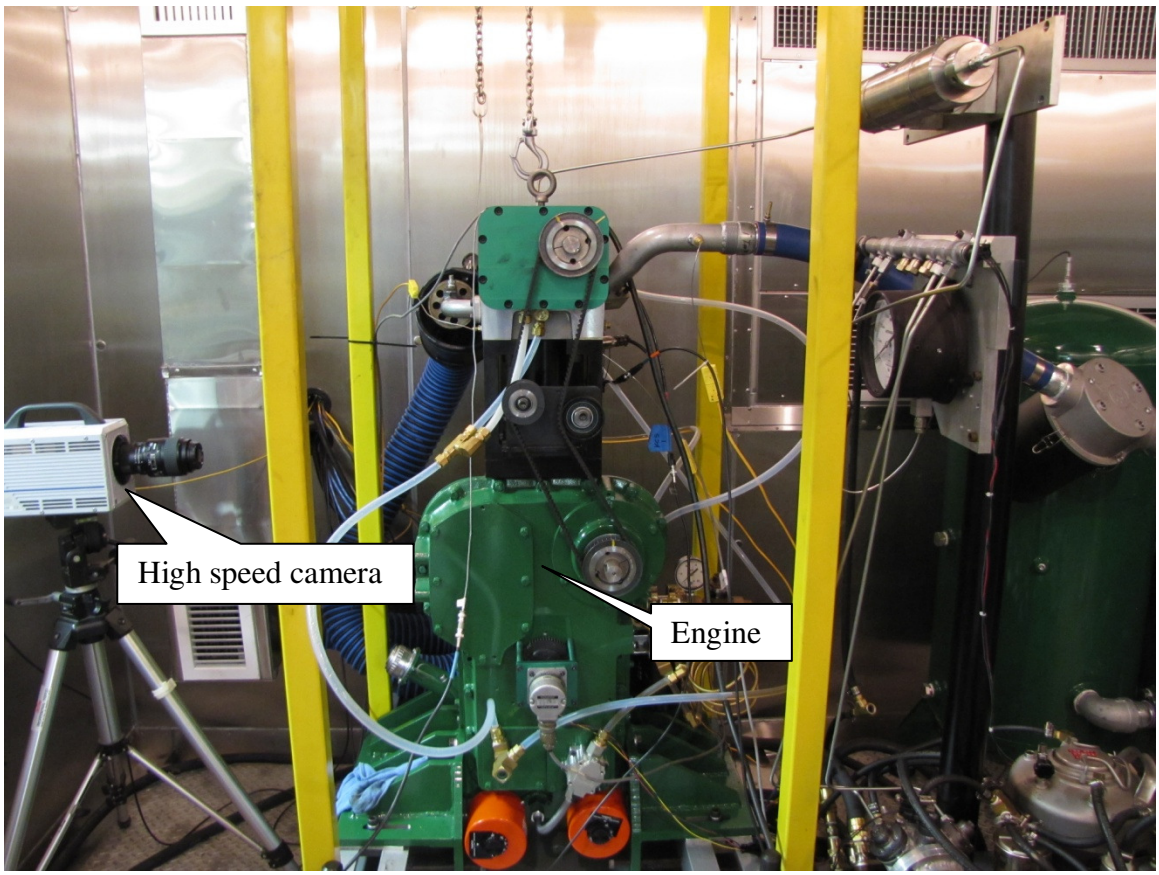

Figure 2-18 Optical diesel engine

Figure 2-18 shows the engine dynamometer test setup of the single cylinder optical diesel engine using the developed control system. The engine was crank-started at several different intake air temperatures. The motivation of this test is to study the affect of the temperature on the diesel fuel evaporation as well as the combustion process. The control system was operated in

the manual mode. Fuel was scheduled to deliver when the engine speed exceeded a threshold (350 rpm in this study). In order to protect the optical engine, a logic that sets number of combustion cycles was designed specifically for this application. The combustion cycles were limited to 30 engine cycles. In addition, a fuel rail pressure control function was added specifically for this application. Two solenoid control channels were provided in the LabVIEW GUI to regulate the fuel pressure in the common rail up to 32,000 psi.

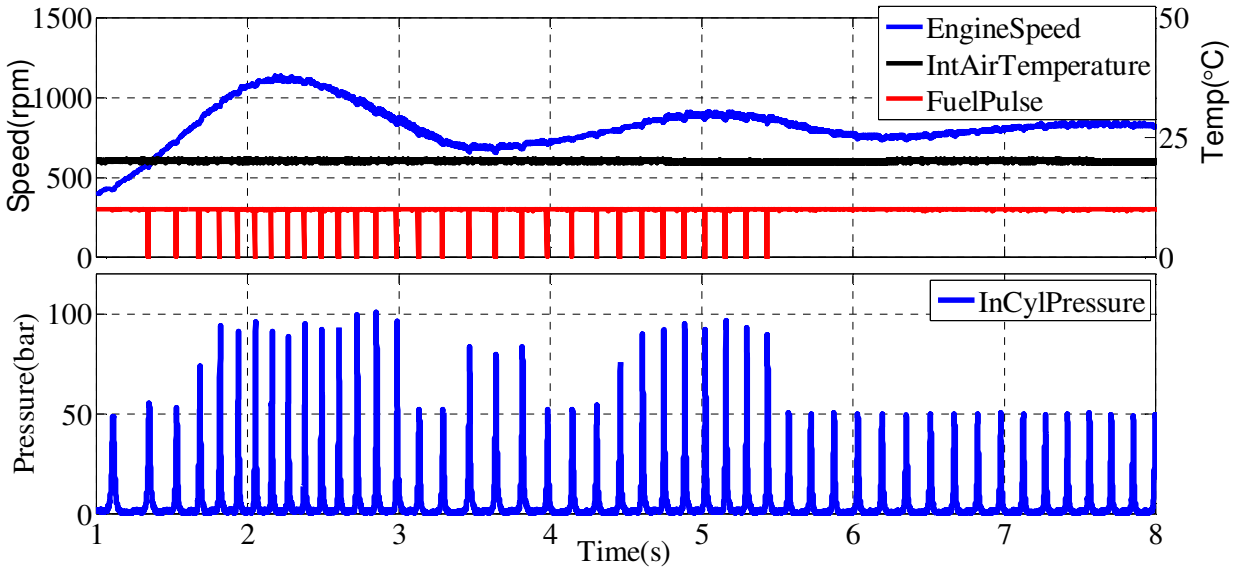

Figure 2-19 Optical diesel engine cold start test

Figure 2-19 shows a cold start test with intake air temperature at 20℃. In this test, a 0.3 ms pilot fuel pulse together with a 0.5 ms main injection pulse were scheduled to deliver at 30 degree BTDC (before top dead center) and 7 degree BTDC, respectively. Base upon the in-cylinder pressure signal (*InCylPressure*), the combustion was observed in the first fuel injection cycle, but it took two engine cycles to get good combustion. Figure 2-20 shows the high speed imaging test of one combustion cycle. The captured images were synchronized with the in-cylinder pressures. The results clearly show the process of the combustion flame development. The visible flame started at 8 degrees after TDC (ATDC), and massive obvious flame appeared

after the peak in-cylinder pressure. The MFB signal in the figure denotes the mass fraction burned that was calculated based upon the method in [36]. In summary, this application proves that the developed engine control system works well in the manual control mode.

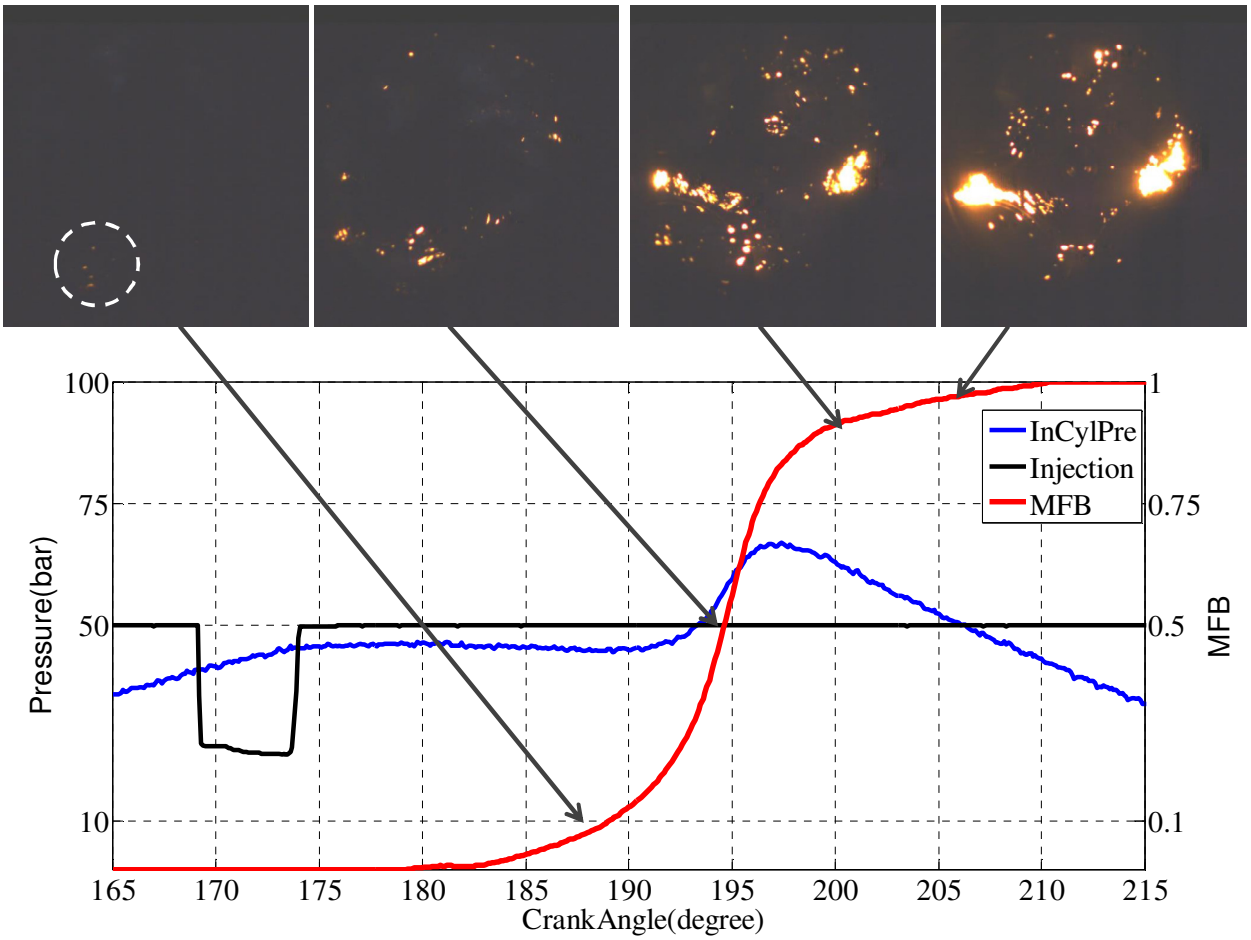

Figure 2-20 Captured flame picture sychronized with the in-cylinder pressure signal

Besides the application to the optical diesel engine, the developed control system was also used for a 4-cylinder gasoline engine. Figure 2-21 shows the control system architecture of the four cylinder engine, where the intake valve system of cylinder 4, originally driven by a CAM shaft, was replaced by a hydraulic valve system (or VVA system). Both the opening and closing timings and lifts of the two VVA valves can be controlled individually. This engine was also tested on an engine dynamometer. This dynamometer can only be used as a resistant load.

The user has to start up the engine and run the engine both in idle and running mode using the developed engine control system. As a result, the developed engine control system starts the engine smoothly, and met all the requirements of the VVA project.

Figure 2-22 shows the test result of the VVA engine controlled by the developed engine control system. The engine was running at 1500 rpm. Two different engine loads, 2.2 bar brake mean effective pressure (BMEP) and 5 bar BMEP were tested for this VVA system. It can be found through the valve profiles that the VVA system worked well, expect that a small surge was found during the closing period of the intake valves. This could be caused by the hydraulic dynamics. But, a conclusion can be safely drawn that the developed engine control system satisfies the requirements of this application.

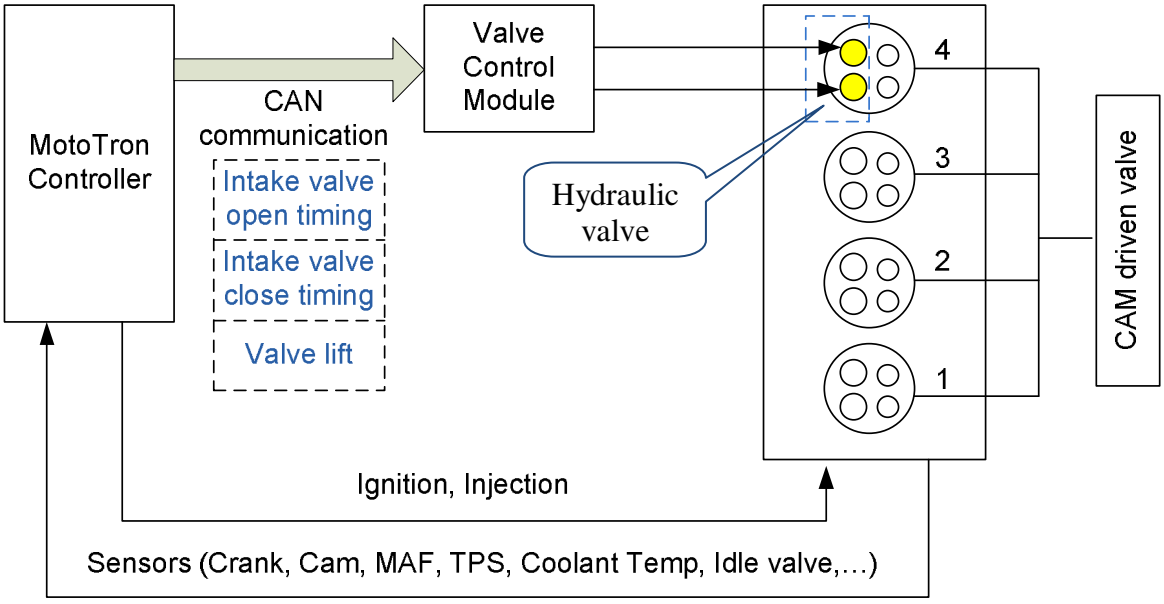

Figure 2-21 Schematic of engine control system with VVA

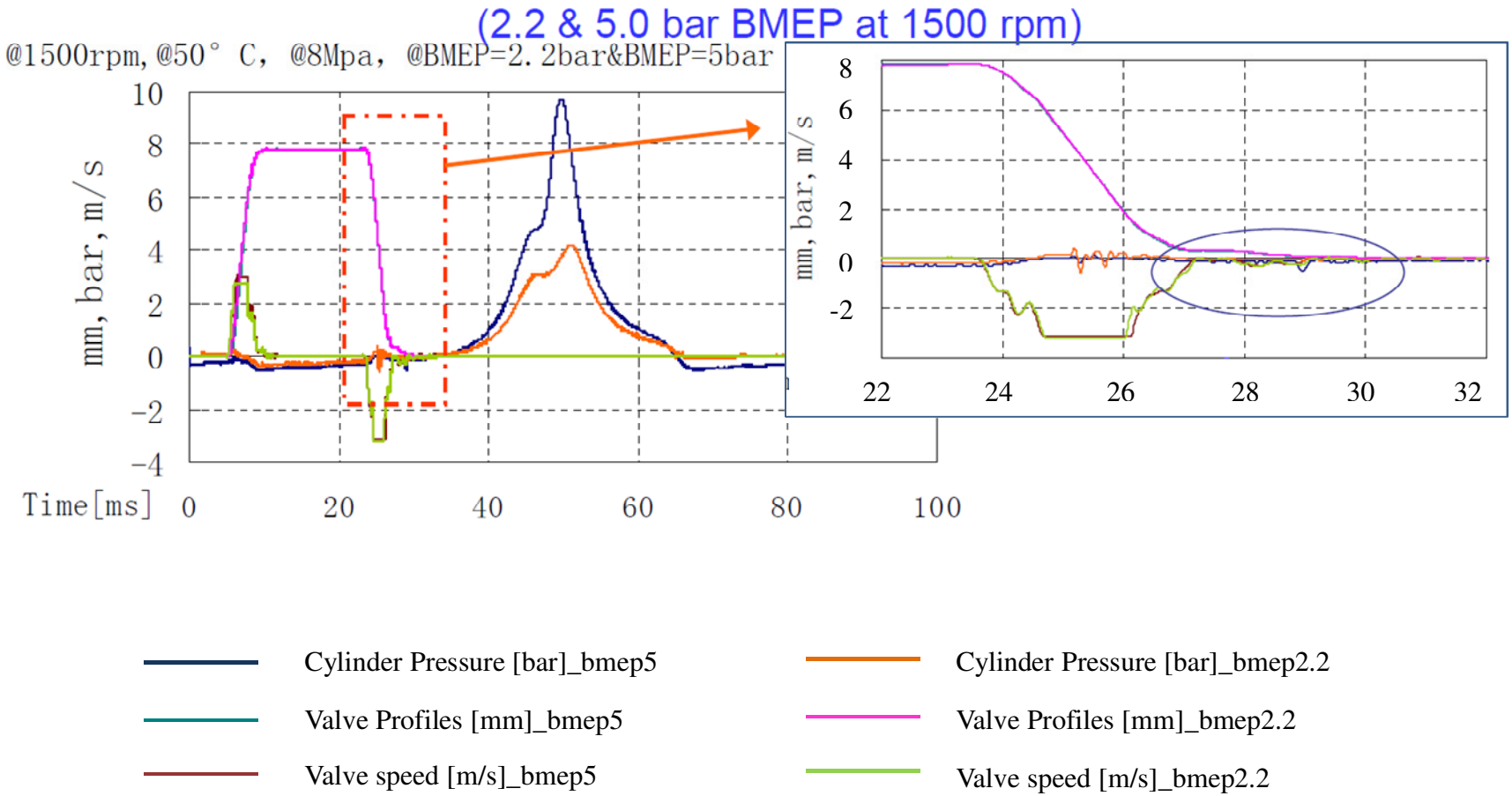

Figure 2-22 Test result of the VVA system

CHAPTER 3

ROBUST FUEL RAIL PRESSURE CONTROL

3.1 Introduction

A steady fuel pressure in the common rail fuel system for diesel engines is always important for accurate fuel metering. However, because common rail fuel systems have complicated fluid dynamics and disturbances from adjacent systems such as the pressure pumps and the fuel injectors, a simple PID controller generally delivers merely satisfactory results [37]. Numerous studies have been devoted to develop more advanced controllers.

In this study, the robust control method was proposed, where the fuel injection was considered as the disturbance input and the fuel viscosity as the system parameter uncertainty. The sensor measurement noise was also taken into consideration in this design. Two robust controllers (H_2 and H_∞ controllers) were developed to regulate the common rail fuel pressure. The performances of the two robust controllers were evaluated by comparing them with a PI baseline controller. The results show that the H_2 controller provided the best performance.

The rest of the chapter is organized as follows. Section 3.2 introduces a common rail fuel system model. In section 3.3, two robust controllers (H_2 controller and H_∞ controller) were developed. The simulation validation results against a PI controller are presented in Section 3.4, and Section 3.5 addresses the conclusions.

3.2 Common Rail Fuel System Modeling

Figure 3-1 depicts a common rail fuel system for a single cylinder diesel engine. The fuel is pressurized through a low-pressure pump and a high-pressure pump. The fuel pressure is regulated by two solenoids, one controls the return line of the high pressure pump, and the other controls the return line of the fuel rail. Both solenoids are default open for safety reason. Fuel returns to the fuel tank through the two solenoids controlled by PWM signals. In this study, both fuel pump motor speeds were fixed. The fuel pump solenoid was also maintained at a constant position by a constant PWM signal. The fuel pressure in the common rail fuel system was regulated by adjusting the opening position of the fuel rail solenoid based upon the feedback fuel pressure sensor signal. The fuel pressure variation is caused by the fuel injection, fuel viscosity change, and so on.

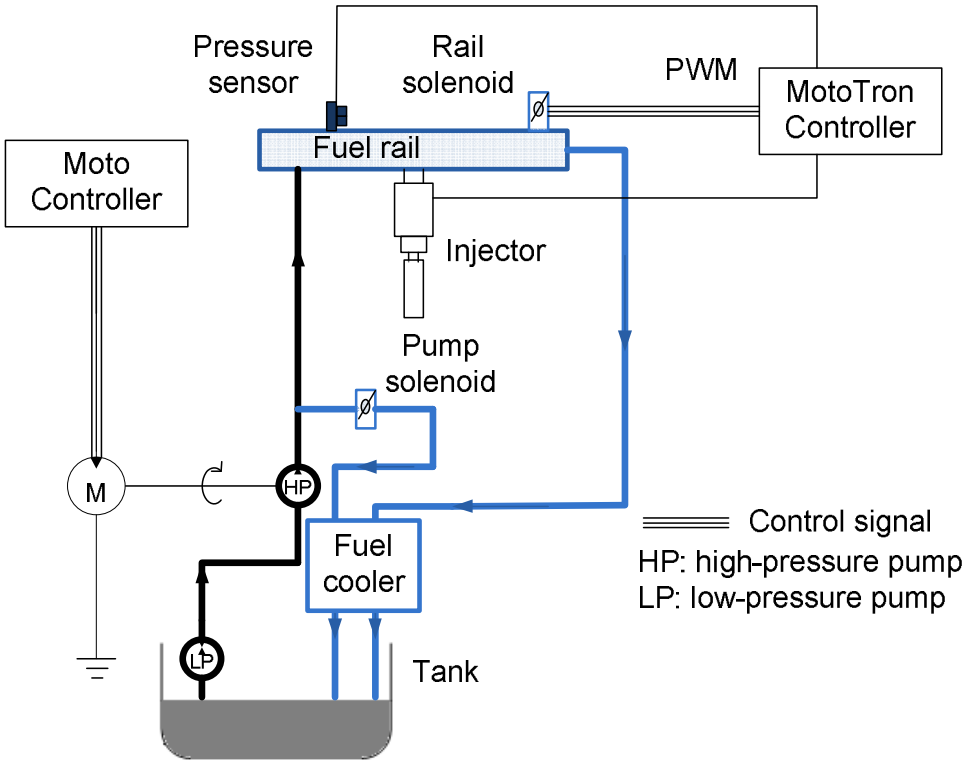

Figure 3-1 Common rail fuel system

3.2.1 Discrete-time mathematic fuel rail model

In this study, the common rail fuel system was modeled as a second-order system. A first order transfer function for the fuel rail solenoid dynamics, and a first order transfer function for the fuel fluid dynamics as shown in (3.1),

$$\frac{Y(s)}{U(s)} = \frac{1}{(\tau_1 s + 1)} \frac{1}{(\tau_2 s + 1)} \tag{3.1}$$

where τ_1 is the time constant of the fuel rail solenoid dynamics, and τ_2 is the time constant for the fuel dynamics. U(s) is the control input (PWM duty cycle signal); while Y(s) is the output fuel rail pressure measured by the pressure sensor.

In a practical application, the fuel dynamics mainly depends on the fuel viscosity, which varies with fuel temperature, and the temperature changes very dramatically when the high pressure fuel pump pressurizes the fuel. Therefore, in this study, an uncertainty parameter δ was introduced into the time constant for fuel fluid dynamics, and the mathematic model with uncertainty can be expressed as follows,

$$\frac{Y(s)}{U(s)} = \frac{1}{(\tau_1 s + 1)} \frac{1}{((\tau_2 + \delta) s + 1)} \tag{3.2}$$

Linear system (3.2) was then discretized into the following discrete transfer function with a sample period of 0.1ms,

$$\frac{Y(z)}{U(z)} = \frac{1-a}{z-a} \frac{1-b}{1-bz^{-1}} \tag{3.3}$$

where $a = e^{-T_S/\tau_1}$, $b = e^{-T_S/\tau_2}(1+\delta)$ (δ is the corresponding uncertainty in discrete domain), and T_S is the sampling time.

3.2.2 LFT of discrete-time system model

Linear fractional transformation (LFT) is a useful method to standardize block diagrams for robust control analysis and design [38]. Figure 3-2 shows the LFT of the discrete-time system model (3-2), where matrix M is a coefficient matrix; W_u, W_y and W_n are dynamic weighting matrices. The weighting matrices were chosen to be first order high-pass filters. Specifically, W_u is used to reflect certain restrictions on the control signals, W_y is used to reflect the requirements on the output, and W_n is used to model the frequency contents of the sensor noise [39]. Signals *d, n, r, u* and *y* represent the fuel injection disturbance, sensor noise, reference fuel pressure, control input, and fuel pressure output, respectively.

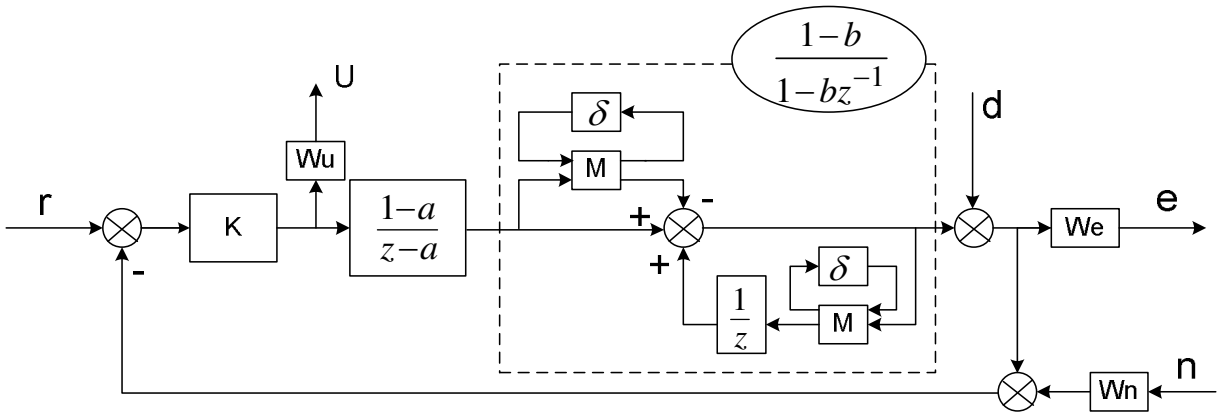

Figure 3-2 System model block diagram

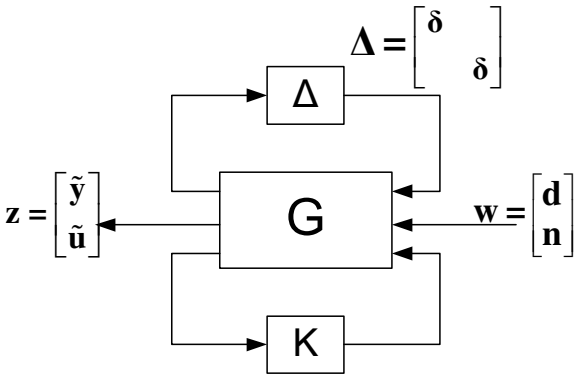

Figure 3-3 General framework

By pulling out the structured uncertainty Δ and the controller K, the system can be reformed into a standard robust control design framework as shown in Figure 3-3. New system input w consists of the disturbance and the sensor noise, and it is defined as

$$w = \begin{bmatrix} d \\ n \end{bmatrix} \tag{3.4}$$

The new system output z consists of the weighted fuel pressure and the weighted solenoid control input, as shown below

$$z = \begin{bmatrix} \tilde{y} \\ \tilde{u} \end{bmatrix} \tag{3.5}$$

Note that, the upper LFT uncertainty matrix Δ is defined as

$$\Delta = \delta I_2 \tag{3.6}$$

The nominal plant G can be expressed in state-space by

$$G = \left[\begin{array}{c|c} A_d & B_d \\ \hline C_d & D_d \end{array}\right] \tag{3.7}$$

where A_d , B_d , C_d , and D_d are state space matrices, and can be implemented in the Matlab/Simulink shown in Figure 3-4.

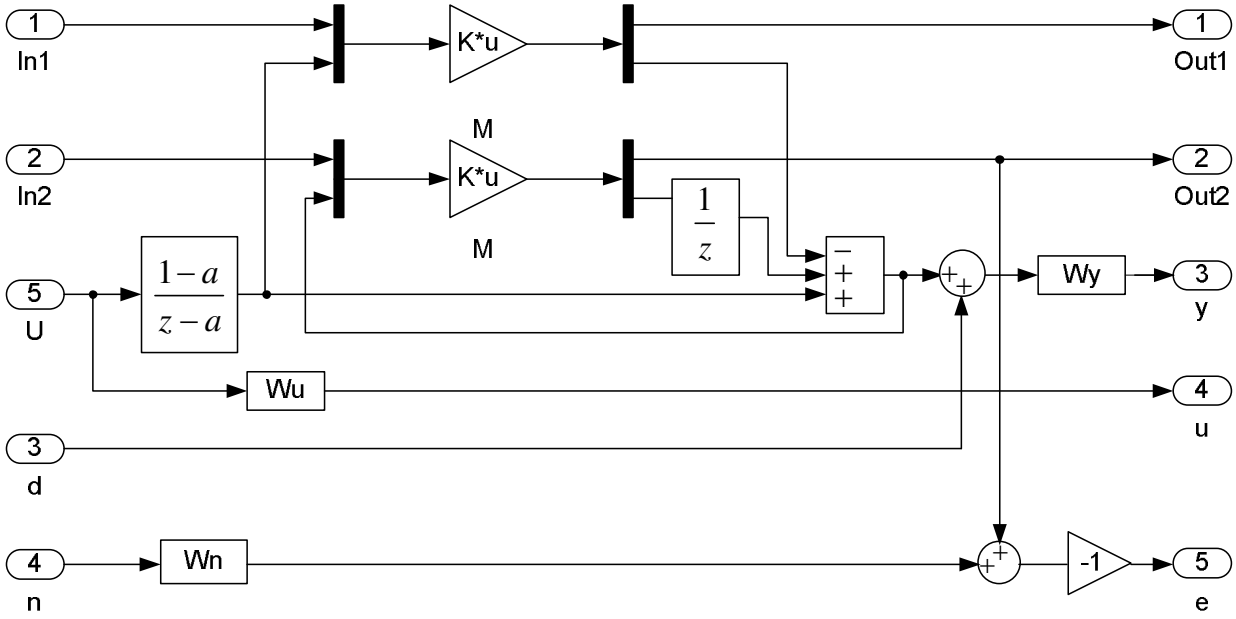

Figure 3-4 Simulink model of G

3.3 Controller Design

Two robust controllers were developed in this study to control the fuel rail pressure subject to injection disturbance, sensor noise and modeling uncertainty. The two controllers are an H_2 controller, and an H_∞ controller. Their performance was evaluated against the baseline PI controller. Figure 3-5 shows the schematic of the fuel rail pressure control system.

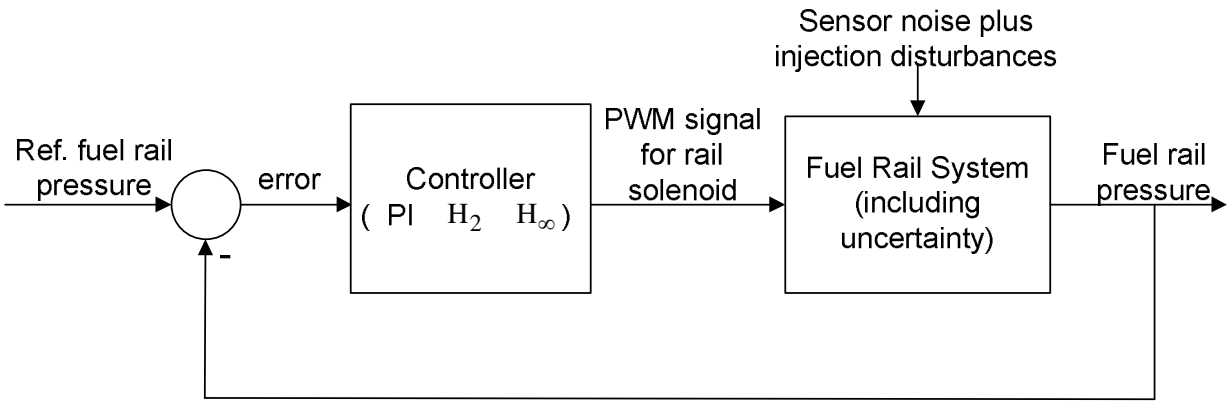

Figure 3-5 Schematic of the fuel rail pressure control system

In this study, the time constant τ_1 was set at 0.01s, and τ_2 was given as 0.001s. Note that, these two values will be calibrated by using the experimental data in the future. The weighting matrices were optimized based upon the controllers' performance and are given in equation (3.8).

$$Wn = \frac{0.05z - 0.0499}{z - 0.9048} \qquad (3.8)$$
$$Wu = \frac{z - 0.9999}{z - 0.999}$$
$$Wy = \frac{2.5}{z - 0.9999999}$$

3.3.1 PI controller

A PI controller was designed as the baseline controller as shown in equation (3.9).

$$U = (K_{fp} + \frac{K_{fI}}{s})(P - r) \qquad (3.9)$$

where U is control input, P is pressure sensor signal, and r is pressure reference signal. The proportional gain K_{fp} and the integral gain K_{fI} in equation (3.9) were optimized by taking into consideration of both control output and control input performance. In this study, K_{fp} is equal to 12.5, and K_{fI} is equal to 4000.

3.3.2 Discrete-time H_2 controller design

The H_2 controller was designed to find a proper, real-rational controller K which stabilizes the plant G internally, and minimizes 2-norm of the transfer matrix T_{zw} from w to z that is defined below

$$\|T_{zw}\|_2^2 = \sup \frac{\|z\|_\infty^2}{\|w\|_2^2} \le \gamma^2 \tag{3.10}$$

where $\|w\|_2^2$ is the square of the 2-norm of the injection disturbance and the sensor noise, $\|z\|_\infty^2$ is the square of the ∞-norm of the input and output, which is calculated as follows,

$$\|z\|_\infty^2 = \sup\begin{bmatrix} \tilde{y}^T & \tilde{u}^T \end{bmatrix}\begin{bmatrix} \tilde{y} \\ \tilde{u} \end{bmatrix} = \sup(\tilde{y}^T\tilde{y} + \tilde{u}^T\tilde{u}) = \sup(y^T W_y^T W_y y + u^T W_u^T W_u u) \tag{3.11}$$

The standard diagram for H_2 controller design is shown below (Figure 3-6).

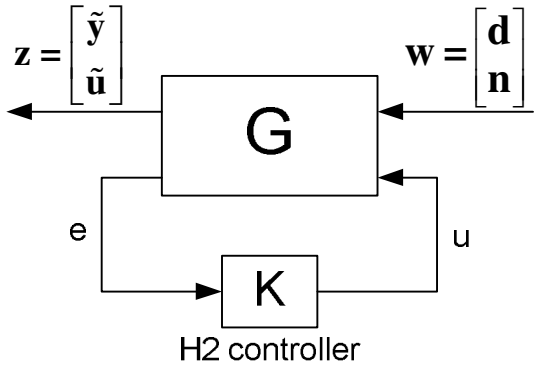

Figure 3-6 Standard block diagram for H_2 controller

The realization of the transfer matrix can be derived directly from the plant G. The optimal H_2 controller K, and the closed-loop transfer matrix T_{zw}, can be calculated using Matlab command "H2SYN". Equation (3.12) provides the controller in its state space representation

$$K = \left[\begin{array}{c|c} A_c & B_c \\ \hline C_c & 0 \end{array}\right] \tag{3.12}$$

where

$$A_c = \begin{bmatrix} 0.8051 & -18.4099 & -2.2778 & 1.9748e-006 & 0 \\ 0.00086 & 0.9048 & 0 & 0 & 0 \\ 1.245e-006 & 0.001308 & 0.9999999 & 0 & 0.004654 \\ -0.1849 & -18.4099 & -2.2778 & 0.999 & 0 \\ -2.541e-005 & -0.0267 & 0 & 0 & 0.9049 \end{bmatrix} \tag{3.13}$$

$$B_c = \begin{bmatrix} -1.214e-017 \\ -2.831e-021 \\ -0.9987 \\ 0 \\ -0.0267 \end{bmatrix}$$

$$C_c = \begin{bmatrix} -0.1849 & -18.4099 & -2.2778 & 1.9749e-007 & 0 \end{bmatrix}$$

and γ is equal to 11.5654.

3.3.3 Discrete-time H_∞ controller design

The H_∞ controller is designed based upon dynamic output-feedback control, with respect to the full order linear dynamic controller

$$\begin{aligned} x_c(k+1) &= A_c x_c(k) + B_c y(k) \\ u(k) &= C_c x_c(k) + D_c y(k) \end{aligned} \tag{3.14}$$

where it is assumed that the controller state $x_c \in \Re^n$.

The theorem in [40] is applied in this design, which is stated as: There exists a controller in the form (3.14) such that the inequality $\left\|T_{zw}(\zeta)\right\|_\infty^2 < \gamma^2$ holds if, and only if, the LMI

$$\begin{bmatrix} P & J & AX+B_uL & A+B_uRC_y & B_u+B_uRD_{yw} & 0 \\ (\bullet)^T & H & Q & YA+FCy & YB_u+FD_{yw} & 0 \\ (\bullet)^T & (\bullet)^T & X+X^T-P & I+S^T-J & 0 & X^TC_z^T+L^TD_{zw}^T \\ (\bullet)^T & (\bullet)^T & (\bullet)^T & Y+Y^T-H & 0 & C_z^T+C_y^TR^TD_{zw}^T \\ (\bullet)^T & (\bullet)^T & (\bullet)^T & (\bullet)^T & I & D_{zw}^T+D_{yw}^TR^TD_{zw}^T \\ (\bullet)^T & (\bullet)^T & (\bullet)^T & (\bullet)^T & (\bullet)^T & \gamma^2 I \end{bmatrix} > 0 \tag{3.15}$$

hold, where the matrices X, L, Y, F, Q, R, S, J and the symmetric matrices P and H are the variables.

According to the theorem, we can get the H_∞ controller as

$$K = \begin{bmatrix} V^{-1} & -V^{-1}YB_u \\ 0 & I \end{bmatrix} \begin{bmatrix} Q-YAX & F \\ L & R \end{bmatrix} \begin{bmatrix} U^{-1} & 0 \\ -C_yXU^{-1} & I \end{bmatrix} \tag{3.16}$$

Using the Simulink/LMILab solver, the H_∞ controller was calculated and given as follows,

$$A_c = \begin{bmatrix} 1.322 & -6.7173e-3 & 0.0233 & 0.166 & 206.2 \\ 77.859 & 0.2235 & 4.168 & 28.75 & 4146 \\ 9.714 & -0.1410 & 1.477 & 3.646 & 610.93 \\ -8.938e-4 & 0 & 0 & 0.999 & 0.0080 \\ 0 & 0 & 0 & 0 & 0.9061 \end{bmatrix} \tag{3.17}$$

$$B_c = \begin{bmatrix} -0.0002076 \\ -0.041739 \\ -0.006150 \\ -8.2567e-9 \\ -1.3724e-9 \end{bmatrix}$$

$$C_c = \begin{bmatrix} -26644.6 & 26.467 & -4.26 & -10390 & -1.8122 \end{bmatrix}$$

3.3.4 Simulation validation for common rail fuel pressure control

In this study, three simulations were desgined for the performance evaluation. The first simulaiton is to compare the tracking performance of the three controllers; the second one is to evaluate the disturbance rejection performance; and the third one is to evaluate the tolerance of the system uncertainty.

Figure 3-7 shows the step response of the three controllers. It is observed that it took the H_2 about 5 ms to converge to the reference value. While the PI controller and H_∞ controller took about 12 ms to converge. Also, the PI controller had the largest overshoot, and used more control input effort than the other two controllers. The H_∞ controller and H_2 controller had close control effort, but the peak value of the control input for H_2 controller is lower than the one of H_∞ controller. This is important for the physical systems which have many input restrictions.

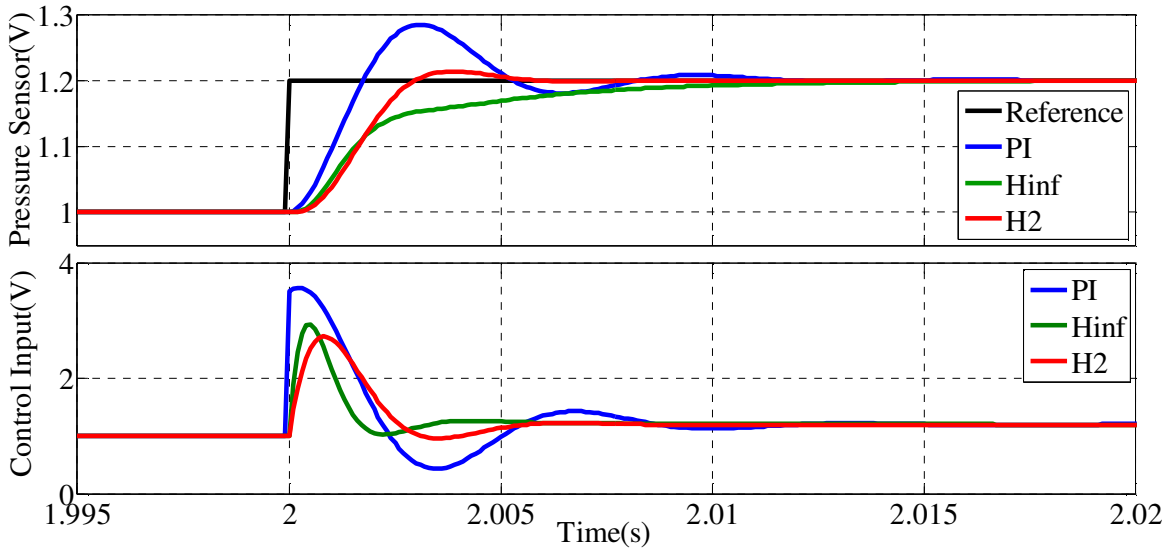

Figure 3-7 Step response comparison of the three controllers

Figure 3-8 shows the response of three different controllers to a pulse distrubance. It can be observed that the H_2 controller obtained the best output performance using least control input effort.

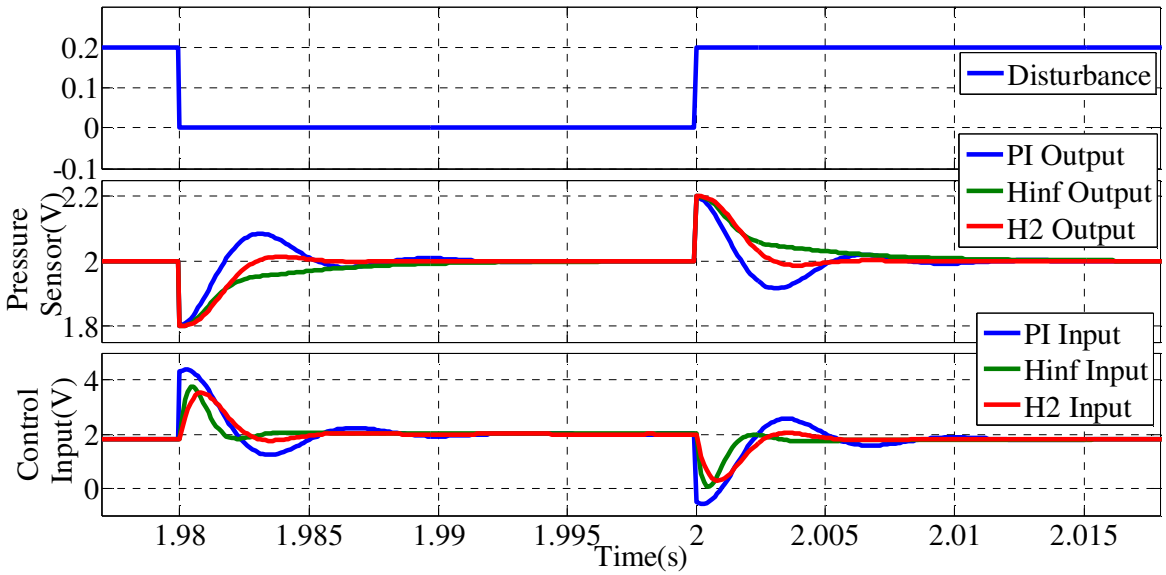

Figure 3-8 Performance comparison of three controllers with step disturbance

The performance of the three controllers responded to the fuel uncertainty is shown in Figure 3-9. In this simulation, a step input was introduced into the plant as the system uncertainty. The simulation results show that H_2 and H_∞ controller has close disturbance tolerance. But H_2 controller converged faster with less control input than H_∞ controller. The PI controller had the worst uncertainty tolerance performance with the most control input request.

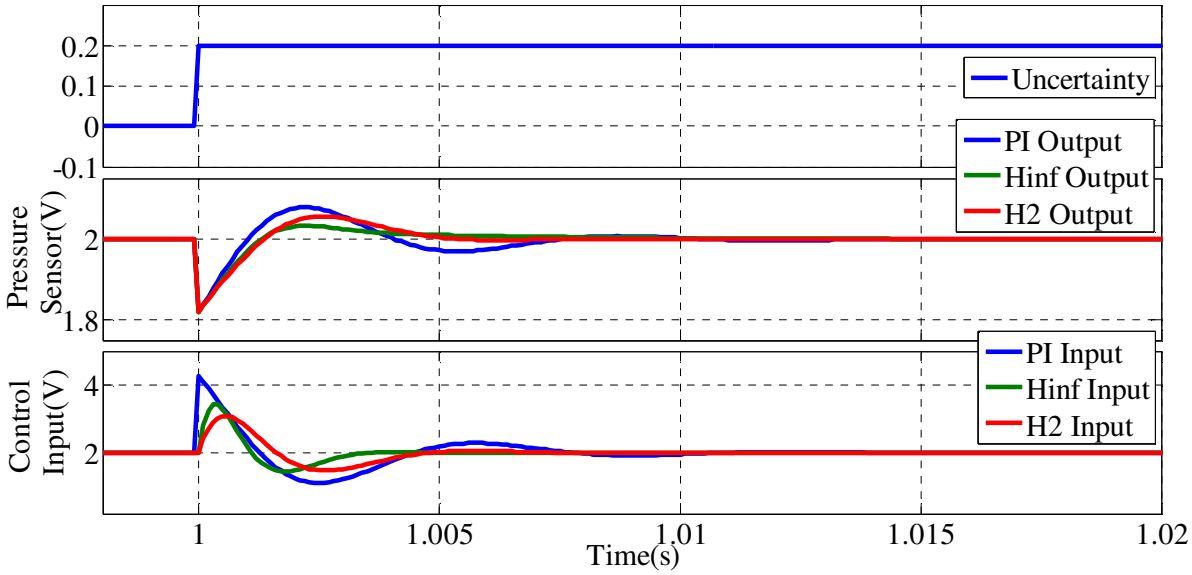

Figure 3-9 Performance comparison of three controllers responded to the fuel uncertainty

Based upon the above results, it can be concluded that the H_2 robust controller required less control input effort while providing better output performance compared with the PI controller and the H_∞ controller. In the future, the control oriented model developed in this study will be calibrated by using the experimental data. Then, the proposed controllers will be optimized and evaluated through experiments.

CHAPTER 4

CONCLUSIONS AND FUTURE WORK

4.1 Conclusions

In this thesis, a prototype engine control system was developed. The control system was developed based upon a MotoTron Controller. A human control interface was also developed using LabVIEW GUI. The MotoTron controller and the host computer communicated through CAN link. The developed engine control system was validated by hardware-in-the-loop (HIL) simulations and used for several engine research projects with different applications, including single and multiple cylinder engines. The results show that the developed engine control system was able to meet the various requirements of the different projects.

In addition, two robust controllers, H_2 and H_∞ controller, were developed to regulate fuel pressure of a common rail fuel system. A PI controller was also developed as a baseline controller for comparison purpose. Three simulations, tracking performance, fuel injection disturbance rejection and fuel uncertainty, were conducted to evaluate the performances of the proposed controllers. The simulation results show that these three controllers had close output performance by optimizing the control gains or weights, but the H_2 controller requires the lease input effort compared to the other controllers.

4.2 Future Recommendations

In this thesis, the developed engine control system was specifically designed for several research engine projects. It can be further improved by adding detailed control logics. In addition, the LabVIEW GUI can also be significantly improved by adding signal displays and control command inputs.

In terms of the proposed robust controllers, it is important to use experimental data to calibrate the control oriented model. Also, it is necessary to optimize the weighting matrices for robust controller design. Lastly, it is suggested to evaluate the proposed controllers through engine dynamometer tests.

BIBLIOGRAPHY

BIBLIOGRAPHY

[1] D. D. Parrish, "Critical Evaluation of US on-road Vehicle Emission Inventories," *Atmospheric Environment*, Vol. 40 (2006) 2288-2300.

[2] W. Harrington, "Fuel Economy and Motor Vehicle Emissions," *Journal of Environmental Economics and Management*, Vol. 33, 240-52 (1997).

[3] R. W. Crandall and J. D. Graham, "The Effect of Fuel Economy Standards on Automobile Safety," *Journal of Law & Economics*, Vol. XXXII (April 1989).

[4] J. H. Boyd and R. E. Mellman, "The Effect of Fuel Economy Standards on the U.S. Automotive Market: An Hedonic Demand Analysis," *Transportation Research*, Vol.14A. pp. 367-378.

[5] P. Bastani, J. B. Heywood, and C. Hope, "US CAFE STANDARDS," (2012).

[6] J. Luo, K. R. Pattipati, L. Qiao, and S. Chigusa, "An integrated diagnostic development process for automotive engine control systems," *Systems, Man, and Cybernetics, Part C: Applications and Reviews, IEEE Transactions* on 37, no. 6 (2007): 1163-1173.

[7] N. Quijano, and K. Passino, "A Tutorial Introduction to Control Systems Development and Implementation with dSPACE," Santhosh Jogi dSPACE Inc. (2002).

[8] A. Monti, S. D'Arco, A. Deshmukh, Y. Work, and A. Lentini, "From simulation to hardware testing: A low-cost platform for Power-Hardware-in-the-Loop experiments," Schindler Electronics Ltd, 6600 Locarno (CH), (2007).

[9] Transportation Research Board Special report 308, "The Safety Promise and Challenge of Automotive Electronics," Transportation Research Board, 2012.

[10] B. R. Suhre, "Mototron Engine Control and Calibration Basics Rev.10," Mototron Corporation. September, 9, 2006.

[11] MotoTron Corp., web site, www.mototron.com.

[12] MotoHawk web site, www.motohawk.info.

[13] Tom Boynton, "General Motors Computerized Vehicle Control System: A Short History", CET249, 2006.

[14] G. Leen, and D. Heffernan, "Expanding automotive electronic systems," *Computer* 35, no. 1 (2002): 88-93.

[15] C. Ursu, R. Bhat, and R. Damodaran, "Simulink Modeling for Vehicle Simulator Design 2011-01-0746," (2011).

[16] C. Salzmann, D. Gillet, and P. Huguenin, "Introduction to real-time control using LabVIEWTM with an application to distance learning," Int. J. Engng Ed 16, no. 5 (2000): 372-384.

[17] G. Stumpp, and M. Ricco, "Common rail: an attractive fuel injection system for passenger car DI diesel engines," *SAE paper* 960870 (1996).

[18] N. Guerrassi, and P. Dupraz, "A common rail injection system for high speed direct injection diesel engines," *SAE technical paper* 980803 (1998).

[19] M. Badami, and P. Nuccio, "Influence of injection pressure on the performance of a DI diesel engine with a common rail fuel injection system," *SAE technical paper*1999-01-0193.

[20] Hk. Suh, HG. Rho, and CS. Lee, "Spray and combustion characteristics of biodiesel fuel in a direct injection common-rail diesel engine," *ASME/IEEE 2007 Joint Rail Conference and Internal Combustion Engine Division Spring Technical Conference (JRC/ICE2007)* March 13–16, 2007 , Pueblo, Colorado, USA.

[21] G. Stumpp, M. Ricco, "Common rail – an attractive fuel injection system for passenger car DI diesel engine," *SAE Technical Paper* 960870, 1996.

[22] D. A. Nehmer, and R. D. Reitz, "Measurement of the effect of injection rate and split injections on diesel engine soot and NOx emissions," *SAE paper* 940668 (1994).

[23] Y. Takeda, N. Ishikawa, M. Komori, and K. Tsujimura, "Diesel Combustion Improvement and Emissions Reduction Using VCO Nozzles with High Pressure Fuel Injection," *SAE Technical Paper* 940899 (1994).

[24] L. Zhang, "A study of pilot injection in a DI diesel engine," *SAE paper* (1999): 01-3493.

[25] P. Lino, B. Maione, and A Rizzo, "Nonlinear modeling and control on a common rail injection system for diesel engines," *Applied Mathematical Modelling*, Vol. 31, 1959, pp. 1770-1784.

[26] R. Morselli, E. Corti, and G. Rizzoni, "Energy based model of a common rail injector," *Proc. of the 2002 IEEE Int. Conf. on Control App*, *Glasgow, Scotland, September 2002*, pp. 1195-1200.

[27] M. Coppo, and C. Dongiovanni, "Experimental validation of a common-rail injector model in the whole operation field," *Journal of Engineering for Gas Turbines and Power*, Vol. 129, 2007, pp. 596-608.

[28] R. Isermann, J. Schaffnit, and S. Sinsel, "Hardware-in-the-loop simulation for the design and testing of engine-control systems," *Control Engineering Practice* 7, no. 5 (1999): 643-653.

[29] H. Hanselmann, "Hardware-in-the Loop Simulation as a Standard Approach for Development, Customization, and Production Test of ECU's," *Society of Automotive Engineers*, 1993.

[30] Z. Lou, "VARIABLE VALVE ACTUATOR," WIPO Patent No. WO/2007/016519, issued February 8, 2007.

[31] JW. Lee, "Variable valve actuator," U.S. Patent Application 12/208,926, filed September 11, 2008.

[32] R. R. Henry, "Single-Cylinder Engine Tests of a Motor-Driven, Variable-Valve Actuator," Society of Automotive Engineers Inc (2001).

[33] T. A. Baritaud, T. A. Heinze, and J. F. Le Coz, "Spray and self-ignition visualization in a DI diesel engine," *SAE paper* NO. 940681, 1994.

[34] J. E. Dec, and R. E. Canaan, "PLIF imaging of NO formation in a DI diesel engine," *SAE paper* 980147, 1998.

[35] J. H. Park, S. Han, and W. H. Kwon, "LQ Tracking Controls with Fixed Terminal States and Their Application to Receding Horizon Controls," *Systems & Control Letters*, Volume 57, Issue 9, Pages 772-777. September 2008.

[36] M.F.J. Brunt, and A.L. Emtage, "Evaluation of burn rate routines and analysis errors," *SAE Paper* No. 970037, 1997.

[37] W. Chatlatanagulchai, T. Aroonsrisopon, and K. Wannaton, "Robust common-rail pressure control for a diesel-dual-fuel engine using QFT-based controller," *SAE Technical Paper* (2009): 01-1799.

[38] K. Zhou, and J. C. Doyle, "Essentials of robust control," Vol. 104. Upper Saddle River, NJ: Prentice Hall, 1998.

[39] K. Zhou, J. C. Doyle, and K. Glover, Robust and Optimal Control, ISBN-13: 978-0134565675, Published by Prentice Hall, August, 1995.

[40] M. C. De Oliveira, J. C. Geromel, and J. Bernussou, "Extended H_2 and H_∞ norm characterizations and controller parameterizations for discrete-time systems," *International Journal of Control* 75, no. 9 (2002): 666-679.